ER-located PIN5 transporter generates potent auxin sinks driven by the IAA decarboxylation pathway

Milada Čovanová, Karel Müller, Nikoleta Klierová, Nayyer Abdollahi Sisi, Petr Skůpa, Ondřej Smetana, Petre Ivanov Dobrev, Kamil Růžička*, Jan Petrášek*

Institute of Experimental Botany, Czech Academy of Sciences, Rozvojová 263, 165 00 Prague 6, Czech Republic

*For correspondence (e-mail kamil.ruzicka@ueb.cas.cz, petrasek@ueb.cas.cz)

The author responsible for distribution of materials integral to the findings presented in this article in accordance with the policy described in the Instructions for Authors (https://academic.oup.com/plphys/pages/General-Instructions) is Jan Petrášek

ER-resided PIN5 triggers IAA decarboxylation and PCD

ABSTRACT

Auxin is an essential and well-investigated regulator of plant development. Still, many aspects determining its (sub-)cellular distribution, as well as its metabolic turnover, are obscure. PIN5 is a transporter that resides on the endoplasmic reticulum and is presumed to influence internal auxin homeostasis by direct sequestration and subsequent degradation. Due to its distinct expression pattern and incomplete metabolomics analyses, the exact role of PIN5 protein and the identity of downstream auxin degradation products show significant gaps. To this end, we utilized morphologically homogeneous tobacco BY-2 cell cultures. We show that the expression of *Arabidopsis thaliana AtPIN5* in the BY-2 system phenocopies so-called auxin starvation defects. Moreover, we reveal that the activity of *At*PIN5 leads, in extreme cases, to the broad range of processes accompanying programmed cell death (PCD). Notably, based on the recently updated knowledge on auxin metabolism, we also show that a significant part of auxin metabolites downstream of the *At*PIN5 activity are part of the re-emerged auxin

decarboxylation pathway. Taking together, we report the direct induction of PCD by auxin stimulus and propose the physiological framework of the auxin decarboxylation route.

INTRODUCTION

The phytohormone auxin, or indole-3-acetic acid (IAA), is vital for plant growth and development. The pattern formation at the level of individual tissues and organs is achieved by the formation of local auxin maxima or minima, orchestrated by the cell-to-cell transport of IAA (Weijers *et al.*, 2021). Among the mediators of auxin flow emerge the transporters of the PIN-formed (PIN) family. Showing a remarkable asymmetrical distribution on the plasma membrane (PM), they coordinate auxin fluxes across the tissues, thereby controlling the downstream developmental programs (Adamowski & Friml, 2015).

Besides the well-investigated auxin fluxes between cells, mediated by the PM-located PINs, another group of PIN proteins was described as residing at the endoplasmic reticulum (ER). The so-called ER-PINs regulate internal auxin levels by conveying auxin into the ER lumen for subsequent metabolization (Mravec *et al.*, 2009; Ding *et al.*, 2012). The metabolic products downstream of the ER-located PIN activity have been examined several times and with various degrees of consistency (Mravec *et al.*, 2009; Ding *et al.*, 2012; Abdollahi Sisi & Růžička, 2020). In addition, the pathways accompanying the IAA breakdown have recently undergone revision (Müller *et al.*, 2021; Hayashi *et al.*, 2021; Dobrev *et al.*, 2023), highlighting the IAA decarboxylation as another relevant auxin degradation route (Bandurski *et al.*, 1995; Dobrev *et al.*, 2023). Thus, many aspects of the IAA homeostasis controlled by ER-PINs remain unclear (Abdollahi Sisi & Růžička, 2020; Ung *et al.*, 2023a).

The connection between auxin and programmed cell death (PCD) has been repeatedly proposed (Kacprzyk *et al.*, 2022). It was shown that auxin pulses produced from the cells undergoing PCD in the outermost layers of the root cap are required for priming lateral root

primordia in the primary root meristem (Xuan *et al.*, 2015, 2016). It was also revealed that auxin can suppress certain instances of PCD (Kerchev *et al.*, 2013). It has even been hypothesized that auxin is a product of tryptophan degradation occurring in defunct cells (Sheldrake, 2021). Nevertheless, the authentic effect of auxin activity to trigger PCD has never been presented.

Cell-suspension cultures have proved to be an excellent model system, which enables studying the effects of growth substances directly and in a homogeneous manner (Petrášek & Zazímalová, 2006; Petrasek *et al.*, 2006). Here, we explore the impact of conditional expression of the well-characterized ER-located *Arabidopsis thaliana At*PIN5 (Mravec *et al.*, 2009) in the BY-2 tobacco suspension cultures. We comprehensively analyze the immediate IAA metabolites downstream of PIN5 activity and reveal the remarkably elevated presence of products of the IAA decarboxylation pathway (Dobrev *et al.*, 2023). We also describe the corresponding phenotypic consequences, including the extreme instances of PCD.

RESULTS

Inducible expression of *At*PIN5 in BY-2 cells phenocopies the symptoms of auxin starvation

The growth and proliferation of tobacco BY-2 cells depends on the exogenous supply of auxin to the media. Its lack is characterized by enhanced cell elongation and lowered cell division, termed collectively as symptoms of auxin starvation (Winicur *et al.*, 1998). We presented earlier that interfering with auxin transport leads to similar morphological defects. The induction of the transgene encoding a PM-located *Arabidopsis thaliana At*PIN7 auxin carrier enhances cell elongation and division arrest, consistent with that occurring on the auxin-free medium (Fig. 1, A to C and Supplemental Fig. S1C; Mravec *et al.*, 2008; Müller *et al.*, 2019). We observed similar auxin-deficient phenotypes by perturbing the nuclear auxin signaling by the inducible expression of the stabilized version of the auxin signaling repressor *At*IAA17, *At*axr3-1 (Leyser *et al.*, 1996; Knox *et al.*, 2003; Figs. 1D-F). We were also able to pharmacologically reduce cell proliferation by the dose-dependent application of IAA antagonist PEO-IAA, which competitively binds the TIR1/AFBs auxin receptors (Nishimura *et al.*, 2009; Fig. S1B). This indicates that the auxin starvation phenotypes are dependent on the TIR1/AFB signaling, in addition to the availability of auxin in the cells.

89 Next, to study the impact of internal auxin fluxes on the cell culture phenotypes, we
90 expressed in the BY-2 cells the characterized *Arabidopsis thaliana* gene *AtPIN5* (Mravec *et al.*,
91 2009; Abdollahi Sisi & Růžička, 2020). We employed two independent transcription inducible
92 systems, XVE (Zuo *et al.*, 2000; Petrasek *et al.*, 2006) and GVG (Aoyama & Chua, 1997; Mravec
93 *et al.*, 2008), triggering the expression of the transgene at the beginning of the subculture
94 interval. Upon the induction of *At*PIN5, the cells became remarkably expanded (Fig. 1G and
95 1H; Supplemental Fig. S1D and S1E), and their cell division reduced (Fig. 1I and Supplemental
96 Fig. S1F), akin to the auxin starvation phenotypes (Fig. 1 A to F and Supplemental Fig. S1C). In
97 addition, the auxin-deficient phenotypes caused by the ER-located *At*PIN5 corresponded to
98 the lowered expression of the auxin reporter *DR5::GFP* (Supplemental Fig. S1G; see also
99 Barbez *et al.*, 2013). This indicates that the *At*PIN5 activity is capable of changing the internal
100 availability of auxin to control the growth and expansion of the BY-2 cells.

101

102 **IAA enhances the symptoms of *At*PIN5-induced auxin starvation**

103 The dependence of the BY-2 tissue cultures on the addition of the synthetic auxin (2,4-
104 dichlorophenoxyacetic acid or 2,4-D) to the media is ascribed to the low levels of endogenous
105 IAA in the cells, caused by its rapid metabolization (Simon *et al.*, 2013; Seifertová *et al.*, 2014;
106 Müller *et al.*, 2021). Accordingly, substituting 2,4-D with IAA also leads to auxin starvation
107 phenotypes (Simon *et al.*, 2013; Fig. 2A). To test the role of internal auxin fluxes under
108 conditions where only native auxin is present, we cultivated the cells expressing *AtPIN5* under
109 the supply of IAA, too. The control lines proliferated less intensively and resembled the auxin-
110 starved ones. Surprisingly, the induction of *At*PIN5 led to even stronger auxin starvation
111 phenotypes (Fig. 2, B and C). Thus, it seems that the PIN5-like transporters can enhance rapid
112 IAA turnover in BY-2 cells.

113 To follow the original idea and to compensate for the fast IAA metabolization more
114 efficiently, we were continuously adding IAA to the media every 12 h during the subcultivation
115 interval. We observed no apparent signs of auxin deficiency (Fig. 2, D and E). Strikingly, though,
116 the *AtPIN5* induction caused strong auxin starvation phenotypes (Fig. 2, D and E). This further
117 underlines that PIN5 is able to generate a potent intracellular IAA sink.

118 ER-PINs are capable of transporting both IAA and 2,4-D (Ung *et al.*, 2022). Hence, we
119 measured the cellular accumulation of radioactively labeled [^{3}H]-IAA and [^{3}H]-2,4-D following

120 the induction of *AtPIN5*. The lines showed a strong cellular uptake of [^{3}H]-IAA (Fig. 2F).
121 Interestingly, we observed no change in the *At*PIN5-mediated [^{3}H]-2,4-D accumulation (Fig.
122 2G). Altogether, our data suggest that *At*PIN5 efficiently channels IAA from the cytosol to be
123 delivered to likely highly active metabolic enzymes inside the ER lumen.
124
125 **Induction of *AtPIN5* promotes programmed cell death**
126 To validate whether the strong auxin withdrawal from the cytosol by *At*PIN5 corresponds
127 to a native downstream process, we analyzed the viability of the cells examined. The trypan
128 blue exclusion test (van Wees, 2008), revealed an increased ratio of cells showing a dye-
129 positive cytoplasm shrinkage as a sign of decreased cell viability following the *At*PIN5 induction
130 (Fig. 3, A and B and Supplemental Fig. S2, A and B). Moreover, the intracellular trypan blue
131 staining was even more apparent in the cells cultured on IAA (Fig. 3, A and B). Thus, the PIN5-
132 mediated funneling of auxin from the cytosol can lead to increased mortality of BY-2 cells.
133 Further, we analyzed the global transcriptional changes downstream of the *At*PIN5 activity
134 to hint at the possible relevant physiological processes related to auxin starvation and lower
135 cell viability. Indeed, using the PANTHER overrepresentation test (Mi *et al.*, 2019), we found a
136 remarkable overlap with the previously published transcriptional profiles from the BY-2 cells
137 cultured in the auxin-free medium (Müller et al., 2021; Fig. 3C and Supplemental Fig. S2, C and
138 D). This included pronounced changes in the expression of stress-related genes, including
139 peroxidases (Supplemental Table S1). We further examined the transcriptional response
140 exclusively linked with the *At*PIN5 expression (Supplemental Table S2), revealing a single
141 enriched gene ontology term (GO:0000041) supported by 6 individual transcripts coding for
142 transporters of transition metals (Peñarrubia *et al.*, 2015). This suggests that the auxin
143 starvation is associated with the enhanced expression of the stress-related peroxidases and
144 that the *AtPIN5* expression leads to the enhanced metal ion transport, presumably activating
145 the response preceding the cell death.
146 The increased expression of peroxidases following the *AtPIN5* induction suggests elevated
147 activity of produced reactive oxygen species (ROS). The role of auxin has been implicated in
148 the crosstalk with ROS homeostasis (Tognetti *et al.*, 2012; Chen *et al.*, 2014b). Hence, we
149 utilized a sensor carboxy-2',7'-dichloro-dihydro-fluorescein diacetate (H2DCFDA), which
150 indicates the intracellular presence of various ROS, including H_2O_2 (Akter *et al.*, 2021). Indeed,
151 upon induction of *AtPIN5*, the cells displayed significantly increased H2DCFDA fluorescence,

152 corroborating the enhanced ROS activity (Fig. 3, D and E and Supplemental Fig. S2E). PIN5 was
153 previously shown to be a part of ER stress adaptive mechanisms (Chen *et al.*, 2014a). Although
154 we did not notice that the repeated additions of IAA into the media would influence the ER
155 localization of *At*PIN5-GFP or lead to remarkable changes in the overall ER structural pattern
156 (Supplemental Fig. S1G and S2F), it was earlier reported that pathways involving ROS
157 production and ER stress are often preceding PCD (Petrov *et al.*, 2015). This thereby further
158 highlights that the lower viability of the *At*PIN5-GFP cells accompanied by ROS can perhaps be
159 ascribed to the initiation of processes related to PCD.

160 Among the main features of PCD are vacuolar leakage and subsequent acidification of
161 cytoplasm (Valandro *et al.*, 2020). To this end, we utilized 2',7'-Bis-(2-carboxyethyl)-5-(and-6)-
162 carboxyfluorescein acetoxymethyl ester (BCECF/AM), a fluorescent dye used for analyzing
163 lowered cytosolic pH as a mark of disrupted vacuolar integrity (Scheuring *et al.*, 2015). Under
164 control conditions, the cells contained several smaller vacuoles. The induction of *At*PIN5 led
165 to the enlargement of central vacuoles, their occasional collapse and acidification of the whole
166 cytoplasm and nucleus (Fig. 3, F and G). Finally, we tested the nuclear DNA fragmentation, a
167 hallmark of PCD, using terminal deoxynucleotidyl transferase-mediated dUTP nick-end
168 labeling (TUNEL) (Tripathi *et al.*, 2017). The expression of *AtPIN5* (Fig. 3, H and I, and
169 Supplemnetal Fig. S3A) resulted in an increased number of TUNEL-stained nuclei, indicating
170 that DNA fragmentation takes part in the signaling cascade downstream of the rapid depletion
171 of auxin in the cytoplasm. However, the decreased cell viability does not appear a general
172 result of deficient auxin response. We also examined the TUNEL signal in cells expressing
173 *AtPIN7* and *Ataxr3-1* in the medium supplemented with IAA in the 12-hour interval. We
174 observed no relevant staining in any of these lines (Supplemental Fig. S3B).

175 We also tested whether the possibly disintegrated cell content can trigger (and enhance)
176 the marks of auxin-induced starvation and PCD. We cultured wild-type BY-2 cells in a medium
177 supplemented with the homogenized cell debris. The cell division rate remained unchanged
178 (Supplemental Fig. S4A), and no obvious signs of increased cell mortality were observed
179 (Supplemental Fig. S4B). This further evidences that the cell death induced by PIN5 expression
180 is a result of the internal cellular activity, rather than being caused by any compound
181 originating from disintegrated cells.

182 Taken together, we conclude that the observed decreased cell viability is associated with
183 PCD, but not uncontrolled stress-related necrotic processes (Van Durme & Nowack, 2016),
184 and it is a specific hallmark of PIN5-madiated auxin starvation.
185

186 **The activity of *At*PIN5 stimulates auxin degradation by the IAA decarboxylation pathway**

187 To get insight into how the ER-mediated IAA conversion affects internal auxin homeostasis
188 in light of recent findings (Müller *et al.*, 2021; Hayashi *et al.*, 2021; Dobrev *et al.*, 2023; Fig.
189 4A), we have tracked the expanded list of IAA metabolites by liquid chromatography-mass
190 spectrometry (LC-MS) following the *AtPIN5* induction. At the time point of adding IAA into
191 media (t_0), its degradation products were barely detectable and their amounts showed
192 negligible differences between the mock and chemical inducer-treated cells (Supplemental
193 Fig. S5A). 2 hours later, we observed that IAA was converted predominantly to amino-acid
194 conjugates of IAA (Fig. 4B; see also Seifertová *et al.*, 2014; Müller *et al.*, 2021; Dobrev *et al.*,
195 2023). The induction of *AtPIN5* usually led to a further increase in IAA conversion in this
196 experimental setup (Fig. 4B and Supplemental Fig. S5B). These measurements illustrate rapid
197 catabolism of IAA in BY-2 cells and evidence that the majority of detected metabolic
198 compounds indeed originate from the supplied IAA.

199 Next, we quantified the IAA breakdown in the cells cultivated in a media supplied with IAA
200 every 12 hours from the beginning of the subcultivation interval. 2 hours after addition, IAA
201 was converted in the control lines into its conjugates as well (Fig. 4C). Surprisingly, the prior
202 induction of *AtPIN5* dramatically reduced the internal IAA levels to close to trace amounts.
203 Although we were also able to detect the activity of the common oxidative IAA degradation
204 pathway, we found remarkably increased conversion towards IAA decarboxylation in these
205 lines (Fig. 4C), as documented by the elevated levels of ascorbigen (Abg) and
206 dihydroascorbigen (DiHAbg) (Dobrev *et al.*, 2023; Fig. 4C). We therefore conclude that the
207 PIN5-mediated auxin sinks are at least partially accompanied by the increased activity of the
208 auxin decarboxylation pathway.

209

210 **The exogenous application of I3C raises the symptoms of cell death in BY-2 cells**

211 It has been proposed earlier that indole-3-carbinol (I3C), an unstable immediate IAA
212 decarboxylation product and precursor of Abg (Fig. 4A) (Hrnčiřík *et al.*, 1998; Chhajed *et al.*,

213 2020; Dobrev *et al.*, 2023), can function as an auxin antagonist and can stimulate vacuolar
214 disintegration and processes related to autophagy in *Arabidopsis* in consequence of the
215 defense reaction (Katz *et al.*, 2015; Katz & Chamovitz, 2017). We therefore incubated the cells
216 with I3C to relate its role to the PIN5-mediated programmed cell death in the BY-2 cultures.
217 Despite the default presence of 2,4-D in the media, I3C treatment affected the cell expansion
218 and proliferation rates (Fig. 5, A and B). I3C also slightly lowered their overall viability (Fig. 5,
219 C and D). However, it remarkably increased the frequency of PCD, as documented by TUNEL
220 staining (Fig. 5, E and F). Taken together, we propose that ER-resided PINs are capable of
221 generating powerful IAA sinks to activate IAA decarboxylation activity and, hereafter,
222 pathways leading to PCD.

223

224 **DISCUSSION**

225 **A possible mechanism underlying PIN5-mediated auxin sinks**

226 The classical concept of polar auxin transport has premised the existence of efflux carriers
227 asymmetrically localized at PM as the central prerequisite for the directional flow of IAA
228 (Rubery & Sheldrake, 1974; Raven, 1975). Later, the PIN auxin transporters were discovered,
229 matching henceforth the proposed attributes of the main IAA carriers (Gälweiler *et al.*, 1998;
230 Petrasek *et al.*, 2006). ER-located PINs were found subsequently, and the relevant works
231 highlighted their capability to influence internal auxin homeostasis (Mravec *et al.*, 2009; Ding
232 *et al.*, 2012; Abdollahi Sisi & Růžička, 2020). Further, the detailed crystallographic studies
233 evidenced that the transporting mechanism employed by both PM and ER-located PINs is
234 identical (Su *et al.*, 2022; Ung *et al.*, 2022; Yang *et al.*, 2022).

235 Yet, many aspects of the PIN-mediated transport remain obscure. Compelling arguments
236 supported by the structural models suggest that IAA is transported from the cytosol against
237 concentration gradients at the expense of membrane potential (Su *et al.*, 2022; Ung *et al.*,
238 2022, 2023a,b; Yang *et al.*, 2022; Andersen *et al.*, 2023). Indeed, in the root apical meristem,
239 PM-located PINs concentrate auxin in the uttermost root tip (Adamowski & Friml, 2015). They
240 also establish and maintain auxin maxima, determining the position of flower primordia in the
241 shoot apical meristem in an equivalent manner (Reinhardt *et al.*, 2003). In contrast, the
242 canalization hypothesis proposes that auxin is funneled away from the site of its external
243 application, i.e., source, towards the sink in the established vascular tissue determining the

244 connective vascular strands (Mitchison, 1980; Sachs, 1991; Ravichandran *et al.*, 2020).
245 Similarly, the root or hypocotyl tropic reactions depend on the transport outwards from the
246 tissue with higher auxin concentration (Friml *et al.*, 2002; Ottenschläger *et al.*, 2003; Rakusová
247 *et al.*, 2011; Band *et al.*, 2012). The expression of PIN5 proteins leads to a remarkable auxin
248 deficiency in BY-2 cells. In the conditions when 2,4-D does not interfere with the internal IAA
249 fluxes (Fig. 5B), the excess of IAA leads to even enhanced PIN5-mediated auxin degradation
250 rates. Hence, in this system, the PIN5-like auxin transporters likely operate in the source-sink
251 mode, too, perhaps by the mechanism of facilitated diffusion, as earlier presumed for auxin
252 canalization (Mitchison, 1980; Rolland-Lagan & Prusinkiewicz, 2005).

253

254 **Auxin metabolization as a prompt for PCD**

255 Along with the auxin-dependent processes, PCD is an inherent part of plant development.
256 The connections between auxin and PCD pathways have been proposed, but mostly indirectly
257 (reviewed in Van Durme & Nowack, 2016; Sheldrake, 2021; Kacprzyk *et al.*, 2022). A chemical
258 screen performed by Kerchev *et al.* (2013) revealed that the H_2O_2-dependent cell death
259 caused by defective photorespiration can be reverted by both synthetic auxins and IAA. Auxin
260 was demonstrated as a central regulator of xylem patterning, where PCD gives rise to
261 conductive vessels (Escamez & Tuominen, 2014; Ruzicka *et al.*, 2015); direct
262 transdifferentiation of the tissue cultures into xylem vessels can also be induced by external
263 cues (Fukuda & Komamine, 1980; Kubo *et al.*, 2005; Ruzicka *et al.*, 2015). In addition, various
264 stages of lateral root development are determined by auxin activity in parallel to PCD
265 (Casimiro *et al.*, 2001; Benková *et al.*, 2003; Swarup *et al.*, 2008; Escamez *et al.*, 2020). Auxin
266 serves as a signal produced by the cells undergoing PCD in the root cap to prime the
267 prospective lateral roots in the primary root meristem (Xuan *et al.*, 2015, 2016). Ultimately, Di
268 Mambro et al. (2019) presented the model that the activity of *PIN5* in the lateral root cap
269 affects root meristem size, but the direct influence of PIN5 on PCD in the lateral root cap has
270 not been investigated.

271 We show that the ER-mediated auxin sinks can trigger PCD in BY-2 cultures. We have not
272 noticed any cells resembling forming xylem vessels following the *AtPIN5* induction. Instead,
273 we report phenotypes associated with common PCD and present lines of evidence that they
274 are linked with the auxin decarboxylation activity. I3C is among native metabolites of

275 glucosinolates, a diverse group of small compounds produced predominantly in *Brassicales*,
276 functioning as agent in the insect defense (Fahey *et al.*, 2001). It is also a product of auxin
277 decarboxylation pathway in a multitude of the (non-)*Brassicales* plant species (Bandurski *et*
278 *al.*, 1995; Kerk *et al.*, 2000; Dobrev *et al.*, 2023). I3C can induce some symptoms of PCD in
279 *Arabidopsis*, in a competitive manner to IAA (Katz *et al.*, 2015; Katz & Chamovitz, 2017). Hence,
280 our data suggest that the two pathways determining PCD overlap and share an unexpectedly
281 common and likely evolutionally conserved functional output.

282

283 **IAA decarboxylation pathway downstream of PIN5-mediated auxin sequestration**

284 PIN5 transports auxin into the ER in order to promote auxin degradation (Mravec *et al.*,
285 2009; Ung *et al.*, 2023a). The levels of IAA-aspartate and IAA-glutamate conjugates are
286 elevated following *At*PIN5 overexpression (Mravec *et al.*, 2009). Paradoxically, the GRETCHEN
287 HAGEN (GH3) enzymes catalyzing the IAA conjugation are generally seen in the cytoplasm
288 (Ludwig-Müller *et al.*, 2009; Ostrowski *et al.*, 2014; Di Mambro *et al.*, 2019; Abdollahi Sisi &
289 Růžička, 2020; Zou *et al.*, 2022). We have recently uncovered a new level of complexity of the
290 IAA metabolome. Among known IAA breakdown routes emerges the auxin decarboxylation
291 pathway, which includes Abg and DiHAbg. Even if occurring across angiosperms, the purpose
292 of auxin decarboxylation is unknown (Dobrev *et al.*, 2023). Strikingly, we found that the
293 relevant metabolic compounds are related to increased AtPIN5 activity. Hence, we conclude
294 that IAA decarboxylation is the main and potent auxin degradation pathway downstream of
295 PIN5.

296

297 **EXPERIMENTAL PROCEDURES**

298 **Plant material, growth conditions and treatments**

299 The tobacco cell lines BY-2 (*Nicotiana tabacum* L., cv. Bright Yellow-2; Nagata *et al.*, 1992)
300 were standardly cultivated in a liquid medium supplemented with 1 µM 2,4-D as described in
301 Petrasek *et al.* (2006) unless stated otherwise. The transformation of cell lines, RT-qPCR
302 validation of the transgene expression, and cell line maintenance were done as described
303 earlier (Petrasek *et al.*, 2006; Müller *et al.*, 2021). By rule, the cells in the exponential growth
304 stage were used, typically 4-d-old, unless specified otherwise.

305 The expression of the *AtPIN7, AtPIN5* and *Ataxr3-1* genes was induced by 1 µM
306 dexamethasone (30 mM stock solution, GVG lines) or 3 µM β-estradiol (30 mM stock solution,
307 XVE lines) at the beginning of the subculture interval. In addition, 2-(1H-indol-3-yl)-4-oxo-4-
308 phenyl-butyric acid (PEO-IAA; OlChemIm, Olomouc, Czech Republic, 10 mM stock solution)
309 and indole-3-carbinol (I3C; Sigma-Aldrich, Merck KGaA, Darmstadt, Germany, 160 mM stock
310 solution) were used. The respective compounds were applied to the cells at the beginning of
311 the subculture interval, and the corresponding amount of the solvent (DMSO) was added to
312 the controls.

313 **Molecular transgenic work**

314 The dexamethasone-inducible gene constructs, *35S>>GVG::AtPIN5* and
315 *35S>>GVG::AtPIN7*, including the corresponding cell cultures, have been described earlier
316 (Petrasek *et al.*, 2006; Mravec *et al.*, 2009). For creating *G10-90>>XVE::AtPIN5*, the
317 corresponding *AtPIN5* open reading frame was cloned with the Gateway system (Invitrogen,
318 Thermo Fisher Scientific, Waltham, MA, USA) into the pMDC7 vector (Curtis & Grossniklaus,
319 2003). The respective Gateway entry clones were generated either by the amplification of
320 wild-type DNA template or that originating from the *PIN5-GFP*^{MGS} plants (Verna *et al.*, 2015)
321 (primer sequences AAAAAGCAGGCTATATGATAAATTGTGGAGAT and
322 AAGAAAGCTGGGTTTCAATGAATAAACTCC). The *XVE::AtPIN5-GFP/DR5::RFP* cell line was
323 obtained by transformation of the *XVE::AtPIN5-GFP* line with the *DR5::RFP* construct (Barbez
324 *et al.*, 2013). The *G10-90>>XVE::Ataxr3-1* line was generated by the transformation of BY-2
325 cells with the construct kindly provided by Jiří Friml.

326 **Microscopy and image analysis**

327 Nomarski differential interference contrast (DIC) microscopy was performed with the
328 Nikon Eclipse E600 microscope (Nikon, Tokyo, Japan) equipped with a color digital camera
329 (DVC 1310C, Austin, Texas, USA). Cell length and diameter were measured manually using the
330 Fiji image analysis software (Rueden *et al.*, 2017). 200 cells in each data set were measured.
331 Cell density was determined by counting the cells with the Fuchs-Rosenthal hemocytometer
332 slide, typically in the fourth day of subcultivation or periodically during the entire period;
333 individual values represent the average of at least six aliquots of every sample. For the
334 fluorescence imaging, Zeiss LSM900 laser scanning microscope (Axio Observer 7, inverted)
335 with Airyscan 2 with Multiplex mode (Carl Zeiss, Jena, Germany) with appropriate filter sets

336 to visualize reporter genes GFP (excitation 488 nm and emission 509 nm wavelengths) and/or
337 mRFP (excitation 590 nm and emission 599 nm wavelengths) was used. Detailed images were
338 obtained with the 40x or 63x water/oil immersion objectives.

339 **Assays on cell viability, ROS content and PCD**

340 The trypan blue exclusion test was used to visualize the penetration of the non-viable cells
341 by the dye (van Wees, 2008). Approximately 10 µl of the 0.4 % trypan blue solution (Sigma-
342 Aldrich) was added to the 0.5 ml cell suspension and recorded subsequently. Cell viability was
343 determined as the percentage of dye-negative cells relative to the total number of cells.

344 For the detection of reactive oxygen species (ROS), the cells were incubated with the 10
345 µM H2DCFDA (2′,7′-dichlorfluorescein-diacetate; Thermo Fisher Scientific, Waltham,
346 Massachusetts, USA) solution (Akter *et al.*, 2021) for 15 min and washed twice with the BY-2
347 medium. The relative ROS accumulation is presented as the mean pixel intensity of cells
348 determined by the Zeiss Zen software. In total, about four hundred cells were counted from
349 three independent experiments. The integrity of the vacuoles was determined after 10 min of
350 staining with 10 µM BCECF-AM ((2′,7′-bis-2-carboxyethyl)-5-(and-6) carboxyfluorescein;
351 Sigma-Aldrich; Scheuring *et al.*, 2015). The number of cells with aberrant vacuolar integrity
352 was assessed as a ratio of cells with the cytoplasmic signal to that of the cells showing a normal
353 vacuolar signal. About five hundred cells were processed in three independent experiments.
354 In both cases, the confocal images were acquired with the Plan-Apochromat 10x/0.45 DIC M27
355 objective.

356 TUNEL (terminal deoxynucleotidyl transferase dUTP nick end labeling) assay (Tripathi *et al.*,
357 2017) was performed in 2-day-old BY-2 cells according to the manufacturer's protocol (TMR
358 red in situ cell death detection kit, Roche Diagnostics GmbH, Heidelberg, Germany) with
359 modifications as described earlier (Smetana *et al.*, 2012). The labeled cells were examined
360 using a color digital camera (DVC 1310C, Austin, Texas, USA) at the Nikon Eclipse E600
361 microscope. All cells were analyzed from at least 10 view fields, covering approximately 100
362 cells each. The quantification is expressed as a percentage of cells carrying the TUNEL signal
363 divided by the total cell number in the visual field. Positive controls, where the samples were
364 additionally treated with DNAse I to detect the positive TUNEL reaction, and negative controls,
365 where the TdT enzyme was omitted from the procedure, were imaged alongside with every
366 experiment.

367 To treat wild-type BY-2 cells with cell debris, one-quarter volume of the total 2-day-old cell
368 culture was collected. The cells were ground with a pestle in a mortar in liquid nitrogen. The
369 homogenized cell content was then washed out by the original medium, and the flowthrough
370 was then returned to the growing cell culture. The cells were subsequently cultivated for two
371 more days before examining their physiological properties.

372 **Auxin uptake assays**

373 Auxin uptake assays were performed in 3-day-old cells as described earlier (Delbarre *et al.*,
374 1996; Petrásek *et al.*, 2003). [^{3}H]-2,4-D (10 Ci.mmol^{-1}) or [^{3}H]-IAA (25 Ci.mmol^{-1}) (American
375 Radiolabeled Chemicals, Inc., St Louis, MO, USA) were added to the equilibrated cell
376 suspension at the beginning of the accumulation assay to the final concentration of 2 nM. The
377 presented values are means of each triplicate from a representative experiment out of three
378 biological repetitions.

379 **IAA metabolic profiling**

380 The harvesting of the 2-d-old BY-2 cells was done 2 hours after the addition of 1 µM IAA
381 into the media, unless stated otherwise. Auxin metabolites were extracted according to
382 previously described procedures (Dobrev & Kamínek, 2002; Dobrev *et al.*, 2023), and
383 determined by the LC-MS quantitative analysis further detailed in Dobrev *et al.* (2023). The
384 samples were processed in triplicates. The results are presented as a mean of at least three
385 independent biological repetitions.

386 **Transcriptome analysis**

387 The total RNA was isolated using RNeasy Plant Mini kit (Qiagen, Düsseldorf, Germany) from
388 50-100 mg of cells cultured in medium for 48 h with IAA added every 12 h, 2 h after the last
389 addition of IAA. Isolated RNA was treated with DNA-Free kit (Thermo Fisher Scientific). RNA
390 purity, concentration and integrity were evaluated on 0.8% agarose gels (v/w) and with the
391 Bioanalyzer RNA Nano 6000 Assay Kit (Agilent Technologies, Santa Clara, CA, USA). RNA
392 sequencing was performed using Illumina NovaSeq 6000 platform. The analysis resulted in at
393 least 15 million 150 bps read pairs. The raw reads were quality-filtered using Rcorrector and
394 Trim Galore scripts (Song & Florea, 2015). Transcript abundances (transcripts per million –
395 TPM) were determined using the Salmon software package (Patro *et al.*, 2017) with
396 parameters --posBias, --seqBias, --gcBias, --numBootstraps 30. The index was built from the

397 *Nicotiana tabacum* v1.0 cDNA dataset (Edwards *et al.*, 2017), by including the *AtPIN5*
398 (*AT5G16530*) gene sequence. Visualization, quality control of data analysis and determination
399 of differentially expressed genes were determined using the sleuth package in R (Love *et al.*,
400 2014; Pimentel *et al.*, 2017) (version 0.29.0). Transcripts with the q-value <= 0.05 and $\log_2$ fold
401 change >=1 (upregulated) or <= -1 (down-regulated) were considered to be significantly
402 differentially expressed. Other criteria for selection of gene list of interest are specified in
403 corresponding result section.

404 Gene ontology analysis (statistical overrepresentation test) was done using the Panther
405 Classification System (Mi *et al.*, 2019). Raw sequencing data are available through GEO Series
406 accession number GSE260945 at the Gene Expression Omnibus
407 (https://www.ncbi.nlm.nih.gov/geo/). The grouping of differentially expressed genes was
408 visualized with the DiVenn software (Sun *et al.*, 2019).

409

410 **ACKNOWLEDGEMENTS**

411 We thank Jiří Friml for kindly providing the *Ataxr3-1* construct, Enrico Scarpella for the *PIN5-*
412 *GFP^{MGS}* lines, Zuzana Vondráková and Nikola Drážná for technical assistance, and Kateřina
413 Malínská for help with image analysis. The work was supported by the Czech Science
414 Foundation (project 19-23773S) to KR, JP and PID. Microscopy was done at the Imaging Facility
415 of the Institute of Experimental Botany and was supported by the Ministry of Education, Youth
416 and Sports of the Czech Republic (LM2023050 Czech-Bioimaging).

417

418 **AUTHOR CONTRIBUTIONS**

419 JP and KR conceived the research. JP, KR and MČ designed the experiments. MČ performed
420 most experiments. KM did RT-qPCR and transcriptome analysis. NK and NAS prepared DNA
421 constructs. PS provided preliminary data essential for the initiation of the study. OS performed
422 part of the PCD assays. PID did metabolic profiling. KR, JP and MČ wrote the manuscript. KR
423 acquired funding. All authors have exercised their right to comment on the manuscript.

424

425 **CONFLICT OF INTEREST**

426 The authors declare no conflict of interest.

427

428 **REFERENCES**

429 **Abdollahi Sisi N, Růžička K**. **2020**. ER-Localized PIN Carriers: Regulators of Intracellular Auxin
430 Homeostasis. *Plants* **9**: 1527.

431 **Adamowski M, Friml J**. **2015**. PIN-Dependent Auxin Transport: Action, Regulation, and Evolution. *The*
432 *Plant Cell* **27**: 20–32.

433 **Akter S, Shahneawz Khan M, N. Smith E, Flashman E**. **2021**. Measuring ROS and redox markers in
434 plant cells. *RSC Chemical Biology* **2**: 1384–1401.

435 **Andersen CG, Bavnhøj L, Pedersen BP**. **2023**. May the proton motive force be with you: A plant
436 transporter review. *Current Opinion in Structural Biology* **79**: 102535.

437 **Aoyama T, Chua NH**. **1997**. A glucocorticoid-mediated transcriptional induction system in transgenic
438 plants. *The Plant Journal: For Cell and Molecular Biology* **11**: 605–612.

439 **Band LR, Wells DM, Larrieu A, Sun J, Middleton AM, French AP, Brunoud G, Sato EM, Wilson MH,**
440 **Péret B, *et al.* 2012**. Root gravitropism is regulated by a transient lateral auxin gradient controlled by
441 a tipping-point mechanism. *Proceedings of the National Academy of Sciences* **109**: 4668–4673.

442 **Bandurski RS, Cohen JD, Slovin JP, Reinecke DM**. **1995**. Auxin biosynthesis and metabolism. In:
443 Davies PJ, ed. Plant Hormones. Physiology, Biochemistry and Molecular Biology. Dordrecht: Springer,
444 39–65.

445 **Barbez E, Laňková M, Pařezová M, Maizel A, Zažímalová E, Petrášek J, Friml J, Kleine-Vehn J**. **2013**.
446 Single-cell-based system to monitor carrier driven cellular auxin homeostasis. *BMC plant biology* **13**:
447 20.

448 **Benková E, Michniewicz M, Sauer M, Teichmann T, Seifertová D, Jürgens G, Friml J**. **2003**. Local,
449 efflux-dependent auxin gradients as a common module for plant organ formation. *Cell* **115**: 591–602.

450 **Casimiro I, Marchant A, Bhalerao RP, Beeckman T, Dhooge S, Swarup R, Graham N, Inzé D,**
451 **Sandberg G, Casero PJ, *et al.* 2001**. Auxin transport promotes Arabidopsis lateral root initiation. *The*
452 *Plant Cell* **13**: 843–852.

453 **Chen Y, Aung K, Rolčík J, Walicki K, Friml J, Brandizzi F**. **2014a**. Inter-regulation of the unfolded
454 protein response and auxin signaling. *The Plant Journal: For Cell and Molecular Biology* **77**: 97–107.

455 **Chen C, Letnik I, Hacham Y, Dobrev P, Ben-Daniel B-H, Vanková R, Amir R, Miller G**. **2014b**.
456 ASCORBATE PEROXIDASE6 Protects Arabidopsis Desiccating and Germinating Seeds from Stress and
457 Mediates Cross Talk between Reactive Oxygen Species, Abscisic Acid, and Auxin. *Plant Physiology*
458 **166**: 370–383.

459 **Chhajed S, Mostafa I, He Y, Abou-Hashem M, El-Domiaty M, Chen S**. **2020**. Glucosinolate
460 Biosynthesis and the Glucosinolate–Myrosinase System in Plant Defense. *Agronomy* **10**: 1786.

461 **Curtis MD, Grossniklaus U**. **2003**. A gateway cloning vector set for high-throughput functional
462 analysis of genes in planta. *Plant Physiology* **133**: 462–469.

463 **Delbarre A, Muller P, Imhoff V, Guern J**. **1996**. Comparison of mechanisms controlling uptake and
464 accumulation of 2,4-dichlorophenoxy acetic acid, naphthalene-1-acetic acid, and indole-3-acetic acid
465 in suspension-cultured tobacco cells. *Planta* **198**: 532–541.

466 **Di Mambro R, Svolacchia N, Dello Ioio R, Pierdonati E, Salvi E, Pedrazzini E, Vitale A, Perilli S,**
467 **Sozzani R, Benfey PN, *et al.* 2019**. The Lateral Root Cap Acts as an Auxin Sink that Controls Meristem
468 Size. *Current Biology* **29**: 1199-1205.e4.

469 **Ding Z, Wang B, Moreno I, Dupláková N, Simon S, Carraro N, Reemmer J, Pěnčík A, Chen X, Tejos R,**
470 ***et al.* 2012**. ER-localized auxin transporter PIN8 regulates auxin homeostasis and male gametophyte
471 development in *Arabidopsis*. *Nature Communications* **3**: 941.

472 **Dobrev PI, Filepová R, Lacek J, Vondráková Z, Müller K, Maršík P, Drašarová L, Talacko P, Hošek P,**
473 **Petrášek J**. **2023**. Study of auxin metabolism using stable isotope labeling and LCMS; evidence for in
474 planta auxin decarboxylation pathway. : 2023.06.02.543384.

475 **Dobrev PI, Kamínek M**. **2002**. Fast and efficient separation of cytokinins from auxin and abscisic acid
476 and their purification using mixed-mode solid-phase extraction. *Journal of Chromatography A* **950**:
477 21–29.

478 **Edwards KD, Fernandez-Pozo N, Drake-Stowe K, Humphry M, Evans AD, Bombarely A, Allen F,**
479 **Hurst R, White B, Kernodle SP, *et al.* 2017**. A reference genome for Nicotiana tabacum enables map-
480 based cloning of homeologous loci implicated in nitrogen utilization efficiency. *BMC Genomics* **18**:
481 448.

482 **Escamez S, André D, Sztojka B, Bollhöner B, Hall H, Berthet B, Voß U, Lers A, Maizel A, Andersson**
483 **M, *et al.* 2020**. Cell Death in Cells Overlying Lateral Root Primordia Facilitates Organ Growth in
484 Arabidopsis. *Current Biology* **30**: 455-464.e7.

485 **Escamez S, Tuominen H**. **2014**. Programmes of cell death and autolysis in tracheary elements: when
486 a suicidal cell arranges its own corpse removal. *Journal of Experimental Botany* **65**: 1313–1321.

487 **Fahey JW, Zalcmann AT, Talalay P**. **2001**. The chemical diversity and distribution of glucosinolates
488 and isothiocyanates among plants. *Phytochemistry* **56**: 5–51.

489 **Friml J, Wiśniewska J, Benková E, Mendgen K, Palme K**. **2002**. Lateral relocation of auxin efflux
490 regulator PIN3 mediates tropism in Arabidopsis. *Nature* **415**: 806–809.

491 **Fukuda H, Komamine A**. **1980**. Establishment of an Experimental System for the Study of Tracheary
492 Element Differentiation from Single Cells Isolated from the Mesophyll of Zinnia elegans. *Plant*
493 *Physiology* **65**: 57–60.

494 **Gälweiler L, Guan C, Müller A, Wisman E, Mendgen K, Yephremov A, Palme K**. **1998**. Regulation of
495 polar auxin transport by AtPIN1 in Arabidopsis vascular tissue. *Science (New York, N.Y.)* **282**: 2226–
496 2230.

497 **Hayashi K, Arai K, Aoi Y, Tanaka Y, Hira H, Guo R, Hu Y, Ge C, Zhao Y, Kasahara H, *et al.* 2021**. The
498 main oxidative inactivation pathway of the plant hormone auxin. *Nature Communications* **12**: 6752.

499 **Hrnčiřík K, Valušek J, Velíšek J**. **1998**. A study on the formation and stability of ascorbigen in an
500 aqueous system. *Food Chemistry* **63**: 349–355.

501 **Kacprzyk J, Burke R, Schwarze J, McCabe PF**. **2022**. Plant programmed cell death meets auxin
502 signalling. *The FEBS Journal* **289**: 1731–1745.

503 **Katz E, Chamovitz DA**. **2017**. Wounding of Arabidopsis leaves induces indole-3-carbinol-dependent
504 autophagy in roots of Arabidopsis thaliana. *The Plant Journal: For Cell and Molecular Biology* **91**: 779–
505 787.

506 **Katz E, Nisani S, Yadav BS, Woldemariam MG, Shai B, Obolski U, Ehrlich M, Shani E, Jander G,**
507 **Chamovitz DA**. **2015**. The glucosinolate breakdown product indole-3-carbinol acts as an auxin
508 antagonist in roots of Arabidopsis thaliana. *The Plant Journal* **82**: 547–555.

509 **Kerchev P, Mühlenbock P, Denecker J, Morreel K, Hoeberichts FA, Van Der Kelen K, Vandorpe M,**
510 **Nguyen L, Audenaert D, Van Breusegem F**. **2013**. Activation of auxin signalling counteracts
511 photorespiratory H2O2-dependent cell death. *Plant, Cell & Environment* **38**: 253–265.

512 **Kerk NM, Jiang K, Feldman LJ**. **2000**. Auxin Metabolism in the Root Apical Meristem. *Plant Physiology*
513 **122**: 925–932.

514 **Knox K, Grierson CS, Leyser O**. **2003**. AXR3 and SHY2 interact to regulate root hair development.
515 *Development (Cambridge, England)* **130**: 5769–5777.

516 **Kubo M, Udagawa M, Nishikubo N, Horiguchi G, Yamaguchi M, Ito J, Mimura T, Fukuda H, Demura**
517 **T**. **2005**. Transcription switches for protoxylem and metaxylem vessel formation. *Genes &*
518 *Development* **19**: 1855–1860.

519 **Leyser HMO, Pickett FB, Dharmasiri S, Estelle M**. **1996**. Mutations in the AXR3 gene of Arabidopsis
520 result in altered auxin response including ectopic expression from the SAUR-AC1 promoter. *The Plant*
521 *Journal* **10**: 403–413.

522 **Love MI, Huber W, Anders S**. **2014**. Moderated estimation of fold change and dispersion for RNA-seq
523 data with DESeq2. *Genome Biology* **15**: 550.

524 **Ludwig-Müller J, Jülke S, Bierfreund NM, Decker EL, Reski R**. **2009**. Moss (Physcomitrella patens)
525 GH3 proteins act in auxin homeostasis. *New Phytologist* **181**: 323–338.

526 **Mi H, Muruganujan A, Ebert D, Huang X, Thomas PD**. **2019**. PANTHER version 14: More genomes, a
527 new PANTHER GO-slim and improvements in enrichment analysis tools. *Nucleic Acids Research* **47**:
528 D419–D426.

529 **Mitchison GJ**. **1980**. A Model for Vein Formation in Higher Plants. *Proceedings of the Royal Society of*
530 *London. Series B, Biological Sciences* **207**: 79–109.

531 **Mravec J, Kubeš M, Bielach A, Gaykova V, Petrášek J, Skůpa P, Chand S, Benková E, Zažímalová E,**
532 **Friml J**. **2008**. Interaction of PIN and PGP transport mechanisms in auxin distribution-dependent
533 development. *Development* **135**: 3345–3354.

534 **Mravec J, Skůpa P, Bailly A, Hoyerová K, Krecek P, Bielach A, Petrásek J, Zhang J, Gaykova V,**
535 **Stierhof Y-D, *et al.* 2009**. Subcellular homeostasis of phytohormone auxin is mediated by the ER-
536 localized PIN5 transporter. *Nature* **459**: 1136–1140.

537 **Müller K, Dobrev PI, Pěnčík A, Hošek P, Vondráková Z, Filepová R, Malínská K, Brunoni F, Helusová**
538 **L, Moravec T, *et al.* 2021**. DIOXYGENASE FOR AUXIN OXIDATION 1 catalyzes the oxidation of IAA
539 amino acid conjugates. *Plant Physiology* **187**: 103–115.

Müller K, Hošek P, Laňková M, Vosolsobě S, Malínská K, Čarná M, Fílová M, Dobrev PI, Helusová M, Hoyerová K, *et al.* 2019. Transcription of specific auxin efflux and influx carriers drives auxin homeostasis in tobacco cells. *The Plant Journal: For Cell and Molecular Biology* **100**: 627–640.

Nagata T, Nemoto Y, Hasezawa S. **1992**. Tobacco BY-2 Cell Line as the "HeLa" Cell in the Cell Biology of Higher Plants. In: Jeon KW, Friedlander M, eds. International Review of Cytology. Academic Press, 1–30.

Nishimura T, Nakano H, Hayashi K, Niwa C, Koshiba T. **2009**. Differential downward stream of auxin synthesized at the tip has a key role in gravitropic curvature via TIR1/AFBs-mediated auxin signaling pathways. *Plant & Cell Physiology* **50**: 1874–1885.

Ostrowski M, Świdziński M, Ciarkowska A, Jakubowska A. **2014**. IAA–amido synthetase activity and GH3 expression during development of pea seedlings. *Acta Physiologiae Plantarum* **36**: 3029–3037.

Ottenschläger I, Wolff P, Wolverton C, Bhalerao RP, Sandberg G, Ishikawa H, Evans M, Palme K. **2003**. Gravity-regulated differential auxin transport from columella to lateral root cap cells. *Proceedings of the National Academy of Sciences* **100**: 2987–2991.

Patro R, Duggal G, Love MI, Irizarry RA, Kingsford C. **2017**. Salmon provides fast and bias-aware quantification of transcript expression. *Nature Methods* **14**: 417–419.

Peñarrubia L, Romero P, Carrió-Seguí A, Andrés-Bordería A, Moreno J, Sanz A. **2015**. Temporal aspects of copper homeostasis and its crosstalk with hormones. *Frontiers in Plant Science* **6**: 255.

Petrásek J, Cerná A, Schwarzerová K, Elckner M, Morris DA, Zazímalová E. **2003**. Do phytotropins inhibit auxin efflux by impairing vesicle traffic? *Plant Physiology* **131**: 254–263.

Petrasek J, Mravec J, Bouchard R, Blakeslee JJ, Abas M, Seifertová D, Wisniewska J, Tadele Z, Kubes M, Covanová M, *et al.* 2006. PIN proteins perform a rate-limiting function in cellular auxin efflux. *Science (New York, N.Y.)* **312**: 914–918.

Petrášek J, Zazímalová E. **2006**. The BY-2 Cell Line as a Tool to Study Auxin Transport. In: Nagata T, Matsuoka K, Inzé D, eds. Biotechnology in Agriculture and Forestry. Tobacco BY-2 Cells: From Cellular Dynamics to Omics. Berlin, Heidelberg: Springer Science & Business Media, 107–118.

Petrov V, Hille J, Mueller-Roeber B, Gechev TS. **2015**. ROS-mediated abiotic stress-induced programmed cell death in plants. *Frontiers in Plant Science* **6**.

Pimentel H, Bray NL, Puente S, Melsted P, Pachter L. **2017**. Differential analysis of RNA-seq incorporating quantification uncertainty. *Nature Methods* **14**: 687–690.

Rakusová H, Gallego-Bartolomé J, Vanstraelen M, Robert HS, Alabadí D, Blázquez MA, Benková E, Friml J. **2011**. Polarization of PIN3-dependent auxin transport for hypocotyl gravitropic response in Arabidopsis thaliana. *The Plant Journal* **67**: 817–826.

Raven JA. **1975**. Transport of indoleacetic acid in plant cells in relation to pH and electrical potential gradients, and its significance for polar IAA transport. *New Phytologist* **74**: 163–172.

Ravichandran SJ, Linh NM, Scarpella E. **2020**. The canalization hypothesis – challenges and alternatives. *New Phytologist* **227**: 1051–1059.

577 **Reinhardt D, Pesce E-R, Stieger P, Mandel T, Baltensperger K, Bennett M, Traas J, Friml J,**
578 **Kuhlemeier C**. **2003**. Regulation of phyllotaxis by polar auxin transport. *Nature* **426**: 255–260.

579 **Rolland-Lagan A-G, Prusinkiewicz P**. **2005**. Reviewing models of auxin canalization in the context of
580 leaf vein pattern formation in Arabidopsis. *The Plant Journal* **44**: 854–865.

581 **Rubery PH, Sheldrake AR**. **1974**. Carrier-mediated auxin transport. *Planta* **118**: 101–121.

582 **Rueden CT, Schindelin J, Hiner MC, DeZonia BE, Walter AE, Arena ET, Eliceiri KW**. **2017**. ImageJ2:
583 ImageJ for the next generation of scientific image data. *BMC Bioinformatics* **18**: 529.

584 **Ruzicka K, Ursache R, Hejátko J, Helariutta Y**. **2015**. Xylem development – from the cradle to the
585 grave. *New Phytologist* **207**: 519–535.

586 **Sachs T**. **1991**. Cell polarity and tissue patterning in plants. *Development* **113**: 83–93.

587 **Scheuring D, Schöller M, Kleine-Vehn J, Löfke C**. **2015**. Vacuolar Staining Methods in Plant Cells. In:
588 Estevez JM, ed. Methods in Molecular Biology. Plant Cell Expansion: Methods and Protocols. New
589 York, NY: Springer, 83–92.

590 **Seifertová D, Skůpa P, Rychtář J, Laňková M, Pařezová M, Dobrev PI, Hoyerová K, Petrášek J,**
591 **Zažímalová E**. **2014**. Characterization of transmembrane auxin transport in Arabidopsis suspension-
592 cultured cells. *Journal of Plant Physiology* **171**: 429–437.

593 **Sheldrake AR**. **2021**. The production of auxin by dying cells. *Journal of Experimental Botany* **72**:
594 2288–2300.

595 **Simon S, Kubeš M, Baster P, Robert S, Dobrev PI, Friml J, Petrášek J, Zažímalová E**. **2013**. Defining
596 the selectivity of processes along the auxin response chain: a study using auxin analogues. *New*
597 *Phytologist* **200**: 1034–1048.

598 **Smetana O, Široký J, Houlné G, Opatrný Z, Chabouté M-E**. **2012**. Non-apoptotic programmed cell
599 death with paraptotic-like features in bleomycin-treated plant cells is suppressed by inhibition of
600 ATM/ATR pathways or NtE2F overexpression. *Journal of Experimental Botany* **63**: 2631–2644.

601 **Song L, Florea L**. **2015**. Rcorrector: efficient and accurate error correction for Illumina RNA-seq reads.
602 *GigaScience* **4**: s13742-015-0089-y.

603 **Su N, Zhu A, Tao X, Ding ZJ, Chang S, Ye F, Zhang Y, Zhao C, Chen Q, Wang J, *et al.* 2022**. Structures
604 and mechanisms of the Arabidopsis auxin transporter PIN3. *Nature* **609**: 616–621.

605 **Sun L, Dong S, Ge Y, Fonseca JP, Robinson ZT, Mysore KS, Mehta P**. **2019**. DiVenn: An Interactive and
606 Integrated Web-Based Visualization Tool for Comparing Gene Lists. *Frontiers in Genetics* **10**: 421.

607 **Swarup K, Benková E, Swarup R, Casimiro I, Péret B, Yang Y, Parry G, Nielsen E, De Smet I, Vanneste**
608 **S, *et al.* 2008**. The auxin influx carrier LAX3 promotes lateral root emergence. *Nature Cell Biology* **10**:
609 946–954.

610 **Tognetti VB, Mühlenbock P, Van Breusegem F**. **2012**. Stress homeostasis – the redox and auxin
611 perspective. *Plant, Cell & Environment* **35**: 321–333.

612 **Tripathi AK, Pareek A, Singla-Pareek SL**. **2017**. TUNEL Assay to Assess Extent of DNA Fragmentation
613 and Programmed Cell Death in Root Cells under Various Stress Conditions. *Bio-Protocol* **7**: e2502.

614 **Ung KL, Schulz L, Kleine-Vehn J, Pedersen BP, Hammes UZ**. **2023a**. Auxin transport at the
615 endoplasmic reticulum: roles and structural similarity of PIN-FORMED and PIN-LIKES. *Journal of*
616 *Experimental Botany*: erad192.

617 **Ung KL, Schulz L, Stokes DL, Hammes UZ, Pedersen BP**. **2023b**. Substrate recognition and transport
618 mechanism of the PIN-FORMED auxin exporters. *Trends in Biochemical Sciences*.

619 **Ung KL, Winkler M, Schulz L, Kolb M, Janacek DP, Dedic E, Stokes DL, Hammes UZ, Pedersen BP**.
620 **2022**. Structures and mechanism of the plant PIN-FORMED auxin transporter. *Nature* **609**: 605–610.

621 **Valandro F, Menguer PK, Cabreira-Cagliari C, Margis-Pinheiro M, Cagliari A**. **2020**. Programmed cell
622 death (PCD) control in plants: New insights from the Arabidopsis thaliana deathosome. *Plant Science*
623 **299**: 110603.

624 **Van Durme M, Nowack MK**. **2016**. Mechanisms of developmentally controlled cell death in plants.
625 *Current Opinion in Plant Biology* **29**: 29–37.

626 **Verna C, Sawchuk MG, Linh NM, Scarpella E**. **2015**. Control of vein network topology by auxin
627 transport. *BMC Biology* **13**: 94.

628 **van Wees S**. **2008**. Phenotypic analysis of Arabidopsis mutants: trypan blue stain for fungi,
629 oomycetes, and dead plant cells. *CSH protocols* **2008**: pdb.prot4982.

630 **Weijers D, Ljung K, Leyser O**. **2021**. *Auxin Signaling: From Synthesis to Systems Biology, Second*
631 *Edition*. Cold Spring Harbor Laboratory Press.

632 **Winicur ZM, Zhang GF, Staehelin LA**. **1998**. Auxin deprivation induces synchronous Golgi
633 differentiation in suspension-cultured tobacco BY-2 cells. *Plant Physiology* **117**: 501–513.

634 **Xuan W, Audenaert D, Parizot B, Möller BK, Njo MF, De Rybel B, De Rop G, Van Isterdael G,**
635 **Mähönen AP, Vanneste S, *et al.* 2015**. Root Cap-Derived Auxin Pre-patterns the Longitudinal Axis of
636 the Arabidopsis Root. *Current Biology* **25**: 1381–1388.

637 **Xuan W, Band LR, Kumpf RP, Damme DV, Parizot B, Rop GD, Opdenacker D, Möller BK, Skorzinski**
638 **N, Njo MF, *et al.* 2016**. Cyclic programmed cell death stimulates hormone signaling and root
639 development in Arabidopsis. *Science* **351**: 384–387.

640 **Yang Z, Xia J, Hong J, Zhang C, Wei H, Ying W, Sun C, Sun L, Mao Y, Gao Y, *et al.* 2022**. Structural
641 insights into auxin recognition and efflux by Arabidopsis PIN1. *Nature* **609**: 611–615.

642 **Zou W, Lin P, Zhao Z, Wang D, Qin L, Xu F, Su Y, Wu Q, Que Y**. **2022**. Genome-Wide Identification of
643 Auxin-Responsive GH3 Gene Family in Saccharum and the Expression of ScGH3-1 in Stress Response.
644 *International Journal of Molecular Sciences* **23**: 12750.

645 **Zuo J, Niu QW, Chua NH**. **2000**. Technical advance: An estrogen receptor-based transactivator XVE
646 mediates highly inducible gene expression in transgenic plants. *The Plant Journal: For Cell and*
647 *Molecular Biology* **24**: 265–273.

648

649 **FIGURE LEGENDS**

650 **Figure 1.** The conditional expression of *XVE::AtPIN5* in BY-2 cells leads to the auxin starvation
651 phenotypes. **A** to **C)** The induction of the *XVE::AtPIN7* transgene results in increased cell
652 elongation **A)**, plotted on **B)** ($P < 0.001$ by Student's *t*-test), and decreased growth, monitored
653 by the cell density in the media **C)**. **D** to **F)** The induction of *XVE::Ataxr3-1* phenocopies the
654 symptoms of auxin starvation documented by representative image on **D)**, quantification of
655 increased cell elongation ($P < 0.001$ by Student's *t*-test) **E)** and reduced proliferation **F)**. **G** to **I)**
656 The induction of *XVE::AtPIN5* in the cell line cultured in a standard medium with 2,4-D leads
657 to increased cell elongation **G)**, plotted on **H)** ($P < 0.05$ by Student's *t*-test), and reduced
658 proliferation rate **I)**. On the dot plots, the open symbols are averages ± S.E. $^{**}P < 0.01$, $^{***}P <$
659 0.001 by Student's *t*-test. Scale bars: 50 µm.

660

661 **Figure 2.** Replacing 2,4-D with its native analog IAA enhances the auxin starvation effects
662 brought about by the induction of *XVE::AtPIN5*. **A)** The comparison of the cell proportions of
663 the control *XVE::AtPIN5* cells cultivated in the medium supplemented with 2,4-D or IAA reveals
664 the increase of the elongation growth in the presence of IAA ($P < 0.001$ by Student's *t*-test). **B**
665 to **C)** The proliferation rate of cells containing the induced *XVE::AtPIN5* transgene is even lower
666 in the medium with IAA added at the beginning of subcultivation, the representative image
667 on **B)**, the corresponding quantification of cell density on **C)**. **D** and **E)** The phenotype of the
668 *XVE::AtPIN5* cells cultured in a medium continuously supplemented with IAA every 12 hours
669 during the monitored cultivation period leads to the partial reversion of the starvation
670 phenotypes in the control lines, however, the induction of the *XVE::AtPIN5* transgene leads to
671 strong auxin starvation phenotypes, as documented at the representative image on **D)** and by
672 the quantification of the cell growth on **E)**. **F** and **G)** The induction of *XVE::AtPIN5* results in
673 higher uptake of [^{3}H]-IAA **F)**, but shows no effect on uptake of [^{3}H]-2,4-D **G)**. Scale bars: 50 µm.
674 On the plots, the open symbols are averages ± S.E. $^{**}P < 0.01$, $^{***}P < 0.001$ by Student's *t*-
675 test.

676

677 **Figure 3.** An increased incidence of symptoms of PCD following induction of *XVE::AtPIN5*. **A**
678 and **B)** The replacement of 2,4-D with IAA leads to more frequent cytoplasm shrinkage and
679 hereafter increased accumulation of the trypan blue dye inside cells (arrowheads), where
680 *XVE::AtPIN5* was induced, as documented by representative images on **A)** and the inverse

681 frequency of the trypan-blue intracellular staining on **B)**. **C)** DiVenn diagram indicating that a
682 large part of differentially expressed genes following the *XVE::AtPIN5* induction is shared with
683 those from the cultures undergoing auxin starvation; red, significantly upregulated genes;
684 blue, downregulated genes; yellow, opposite expression changes. A single dot denotes a group
685 of 10 genes. **D** and **E)** An increased fluorescence intensity on confocal images of the H2DCFDA
686 staining of *XVE::AtPIN5* lines detects an elevated presence of ROS following the transgene
687 induction **D)**, as quantified in **E)**. **F** and **G)** Confocal images of cells stained by BCECF-AM to
688 mark acidic areas **F)**, as quantified in **G)**, document that the *XVE::AtPIN5* induction leads to
689 decreased acidity in vacuoles but increased acidity in the cytoplasm and nucleus area
690 (arrowheads). **H** and **I)** Representative images of TUNEL staining, marking the disintegration
691 of nuclear DNA (red channel: TUNEL, blue channel: nuclear DAPI staining) **H)**, shows an
692 enhanced labeling frequency in the lines where *XVE::AtPIN5* was induced **I)**. For **D)** and **F)**, the
693 color intensity is indicated by the rainbow color lookup table (inset on **D)**). Scale bars: 50 µm.
694 On the dot plots, the open symbols are averages ± S.E. **P* < 0.05, ***P* < 0.01, ****P* < 0.001 by
695 Student's *t*-test.
696
697 **Figure 4.** Inducible *XVE::AtPIN5* expression in BY-2 cells promotes IAA deactivation by the
698 decarboxylation pathway. **A)** A scheme of current understanding of main IAA degradation
699 pathways (products of IAA oxidation pathway in blue, IAA decarboxylation in red). **B)** LC-MS
700 quantification of IAA and its metabolites in the cells expressing *XVE::AtPIN5* cultured on the
701 standard 2,4-D-supplemented media shows a moderate decrease of IAA and its most
702 degradation products. **C)** The induction of *XVE::AtPIN5* in the cells cultivated in media with IAA
703 added every 12 hours leads to a dramatic drop of IAA and its conjugates, while the compounds
704 belonging to the IAA decarboxylation pathway show elevated levels. On **B)** and **C)**, the open
705 symbols indicate the mean from three independent measurements; the bars are ± S.E. **P* <
706 0.05, ***P* < 0.01, ****P* < 0.001, by Student's *t*-test, n. s.: not significant at $\alpha_{0.05}$. IAA: indole-3-
707 acetic acid, IAA-Asp: IAA-aspartate, IAA-GE: IAA-glucose ester, OxIAA-Asp: Oxo-IAA-aspartate,
708 Abg: ascorbigen, DiHAbg: dihydroascorbigen, I3M-SG: indole-3-methylglutathione. The cells
709 were harvested 2 hours after the addition of 1 µM IAA.
710
711 **Figure 5.** The I3C treatment leads to growth arrest and reduced viability of BY-2 cells. **A)** The
712 addition of 50 µM I3C to the media leads to increased elongation of BY-2 cells (*P* < 0.001 by

713 Student's *t*-test) and **B)** decreased proliferation, monitored by the cell density in the media. **C**
714 to **F)** The I3C treatment also results in increased cell mortality monitored by trypan blue **C** and
715 **D)** and TUNEL staining (red channel: TUNEL, blue channel: nuclear DAPI staining) **E** and **F)**.
716 Scale bars: 50 µm. On the dot plots, the open symbols are averages ± S.E. ***$P < 0.001$ by
717 Student's *t*-test.
718
719 **SUPPLEMENTAL FIGURE LEGENDS**
720 **Figure S1.** Additional aspects of auxin deficiency of tobacco BY-2 cells. **A)** The induction of the
721 *GVG::AtPIN7* transgene leads to decreased cell density, reflecting their lower proliferation rate
722 during the whole subcultivation interval. **B)** The cell density of the wild-type BY-2 cells
723 decreases with the growing concentration of supplied PEO-IAA, an inhibitor of auxin-
724 dependent gene expression ($F(5,48) = [11.112]$, $P < 0.001$ by one-way ANOVA). **C)** The enhanced
725 cell expansion is typical for cultivation on the auxin-free medium (shown on the *GVG::AtPIN7*
726 line without the chemical inducer). **D** to **F)** The conditional expression of *GVG::AtPIN5* in the
727 cell lines cultured in standard medium with 2,4-D leads to increased cell expansion **D** and **E)**
728 ($P < 0.001$ by Student's t-test) and reduced proliferation rates **F)**. **G** to **H)** The induction of
729 *XVE::AtPIN5-GFP* in the cells co-expressing auxin *DR5::RFP* reporter results in a reduction of
730 the fluorescence in cells in the upper-intensity quantiles **G)**, and PIN5-GFP colocalizes with the
731 ER-targeted RFP **H)**. On **A)**, **B)** and **F)**, the open symbols are averages ± S.E. On **G)**, the vertical
732 error bars represent median ± 95% confidence intervals. Scale bars: 50 µm on **C)**, **D)** and **H)**.
733
734 **Figure S2.** Increased frequency of symptoms of cell death and its relationship to auxin
735 starvation following induction of *AtPIN5*. **A** and **B)** The representative images of incorporation
736 of the trypan blue inside the cells following induction of *GVG::AtPIN5* **A)**, quantified on **B)**. **C**
737 and **D)** Quality control of RNA-Seq data processing, a heat-map representing Jensen-Shannon
738 divergence between individual samples (sorted by internal sample IDs) **C)**, projections of
739 individual samples onto the principal components (PC) **D)**. **E)** An increased fluorescence on
740 confocal images of the *GVG::AtPIN5* cells stained by 10 µM H2DCFDA to detect ROS, following
741 the transgene induction. **F)** The pattern and intensity of the *At*PIN5-GFP foci are comparable
742 in both standard 2,4-D-containing medium and that continuously supplemented with IAA
743 every 12 hours. The signal intensity is indicated by the green fire blue rainbow lookup table
744 on **F)**. On **B)**, the dot plot of a data set of 2000 cells in total, the open symbols are averages ±

745 S.E. , ***$P < 0.001$ by Student's *t*-test. Scale bars: 25 µm on **A)**, 100 µm on **E)**, and 10 µm on
746 **F)**.
747
748 **Figure S3.** Detection of the DNA fragmentation during auxin deficiency. **A)** TUNEL staining (left:
749 TUNEL, middle: control nuclear DAPI staining, right: merged false-colored images) marks an
750 enhanced disintegration of nuclear DNA in the cells where *GVG::AtPIN5* was induced. **B** to **C)**
751 Negative TUNEL stainings in *GVG::AtPIN7* and *XVE::Ataxr3-1* cells evidence the absence of the
752 PCD, both under the standard conditions **B)**, or when supplemented with IAA every 12 hours
753 during the monitored cultivation period **C)**. Upper panels: control nuclear DAPI staining, lower
754 panels: TUNEL. Ctrl (+): control cells additionally treated with DNAse I to detect the positive
755 TUNEL reaction, Ctrl (-): staining where the TdT enzyme action was omitted from the control
756 reaction. Scale bars: 50 µm.
757
758 **Figure S4.** WT BY-2 cells cultured in a medium containing cell debris exhibit neither decrease
759 of proliferation activity **A)** nor signs of decreased viability monitored by trypan blue staining
760 **B)**. Scale bar: 100 µm on **B)**.
761
762 **Figure S5.** Additional experiments examining the activity of the IAA decarboxylation pathway
763 following the *AtPIN5* expression. **A)** Representative LC-MS analysis of IAA and its metabolites
764 in cells expressing *XVE::AtPIN5* determined immediately after 1 µM IAA supply (t_0). While the
765 exogenously applied IAA is up-taken immediately, the levels of its metabolites are still barely
766 detectable. **B)** LC-MS analysis of IAA and its metabolites in cells expressing *GVG::AtPIN5*
767 cultured on the standard 2,4-D-supplemented media, 2 hours after adding 1 µM IAA. Open
768 symbols indicate the mean of three technical measurements; the bars are ± S.E. **$P < 0.01$,
769 ***$P < 0.001$ by Student's *t*-test, n. s.: not significant at $\alpha_{0.05}$. IAA: indole-3-acetic acid, IAA-
770 Asp: IAA-aspartate, IAA-GE: IAA-glucose ester, OxIAA-Asp: Oxo-IAA-aspartate, Abg:
771 ascorbigen, DiHAbg: dihydroascorbigen.
772
773
774 **Table S1.** Results of PANTHER Overrepresentation test (GO - Molecular function) of transcripts
775 significantly upregulated in both auxin-starved and the *XVE::AtPIN5*-expressing cells.
776

777 **Table S2.** Results of PANTHER Overrepresentation test (GO - Molecular function) of transcripts
778 significantly upregulated in BY-2 cells carrying induced *XVE::AtPIN5*, compared to untreated
779 controls and auxin-starved cells.

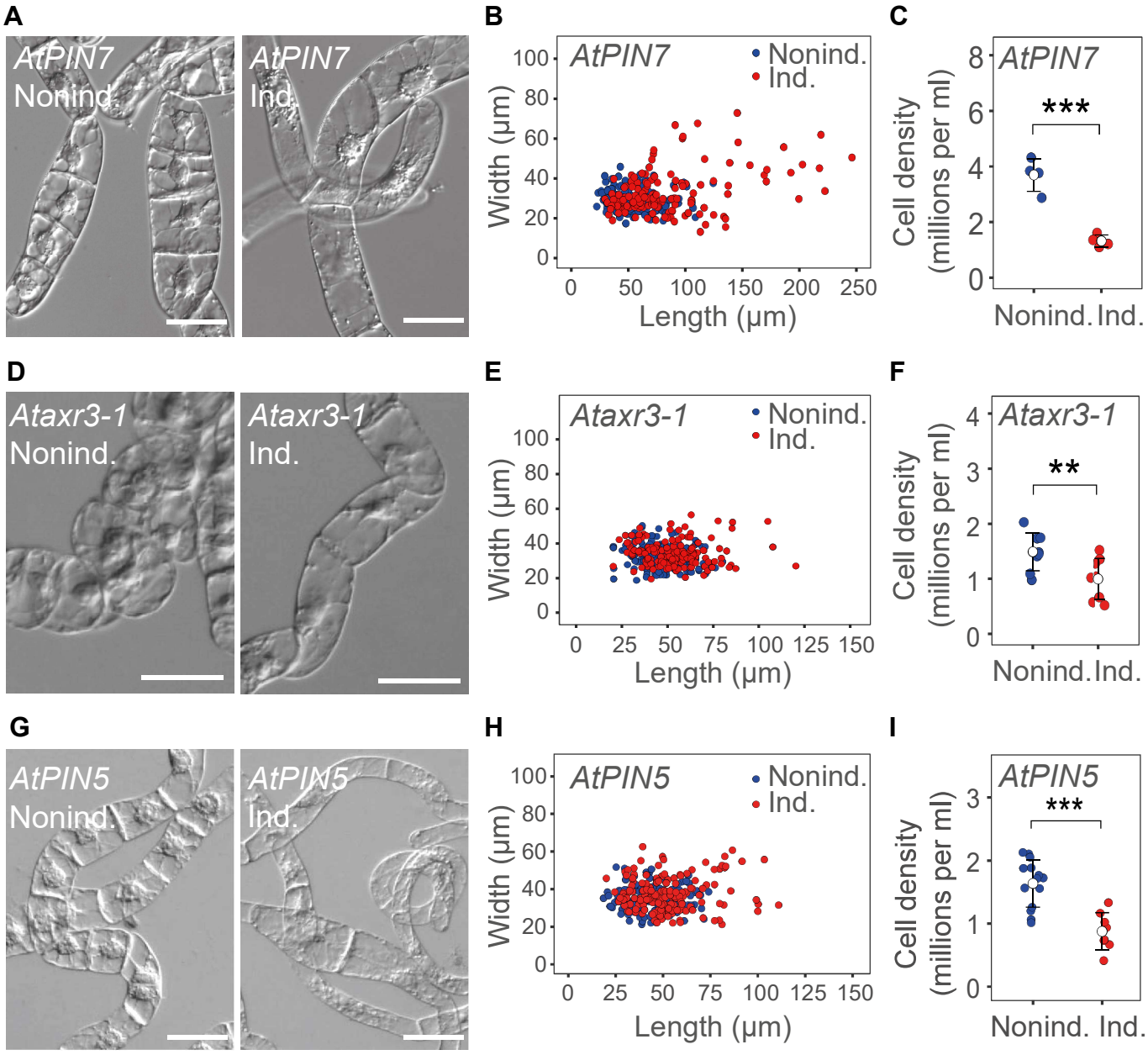
A
AtPIN7
Nonind.
AtPIN7
Ind.
B
AtPIN7
Nonind.
Ind.
Width (µm)
Length (µm)
C
AtPIN7
***
Cell density (millions per ml)
Nonind.
Ind.
D
Ataxr3-1
Nonind.
Ataxr3-1
Ind.
E
Ataxr3-1
Nonind.
Ind.
Width (µm)
Length (µm)
F
Ataxr3-1
**
Cell density (millions per ml)
Nonind.
Ind.
G
AtPIN5
Nonind.
AtPIN5
Ind.
H
AtPIN5
Nonind.
Ind.
Width (µm)
Length (µm)
I
AtPIN5
***
Cell density (millions per ml)
Nonind.
Ind.

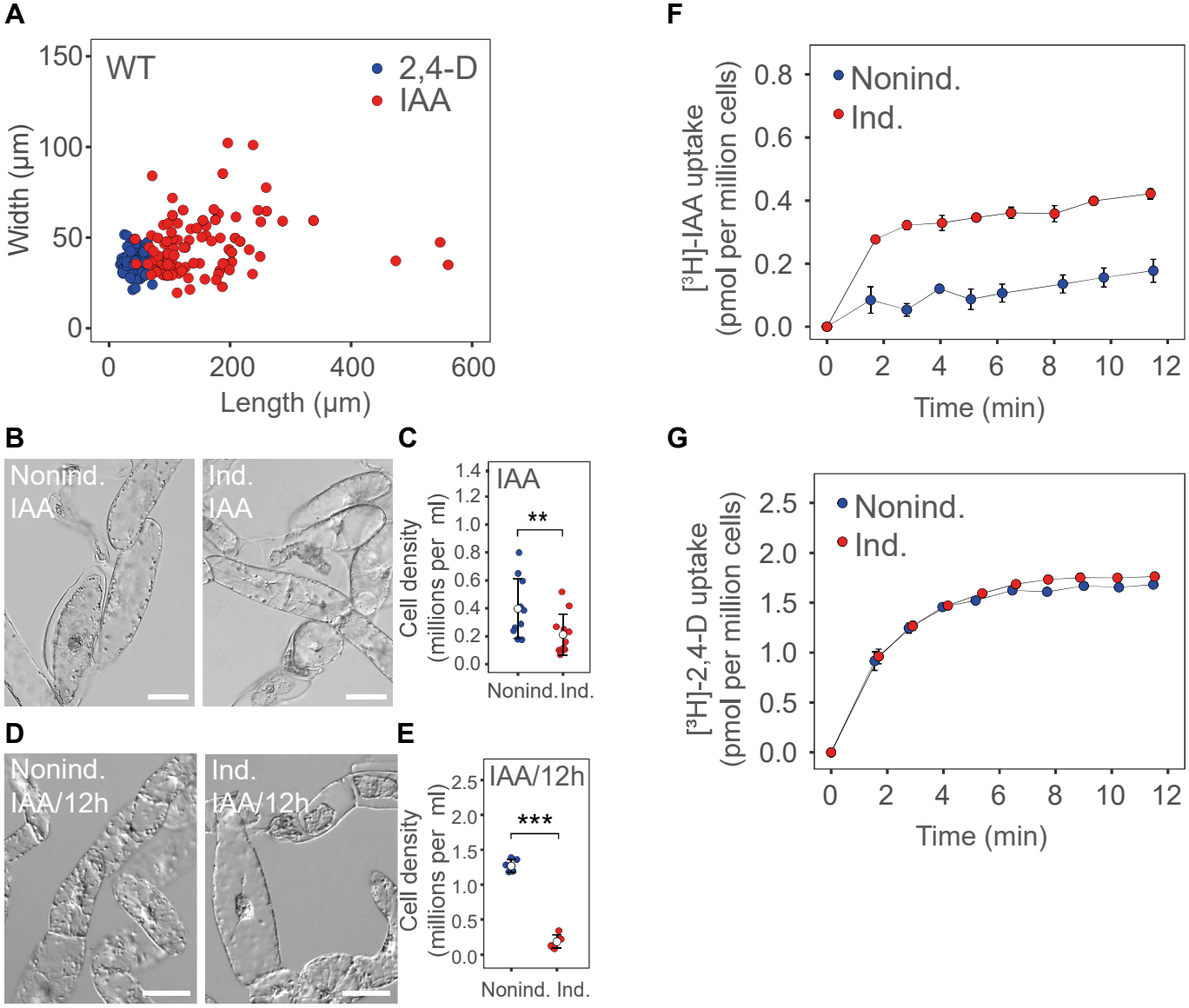
A
WT
2,4-D
IAA
Width (µm)
Length (µm)
B
Nonind.
IAA
Ind.
IAA
C
IAA
Cell density
(millions per ml)
Nonind.
Ind.
D
Nonind.
IAA/12h
Ind.
IAA/12h
E
IAA/12h
Cell density
(millions per ml)
Nonind.
Ind.
F
Nonind.
Ind.
[3H]-IAA uptake
(pmol per million cells)
Time (min)
G
Nonind.
Ind.
[3H]-2,4-D uptake
(pmol per million cells)
Time (min)

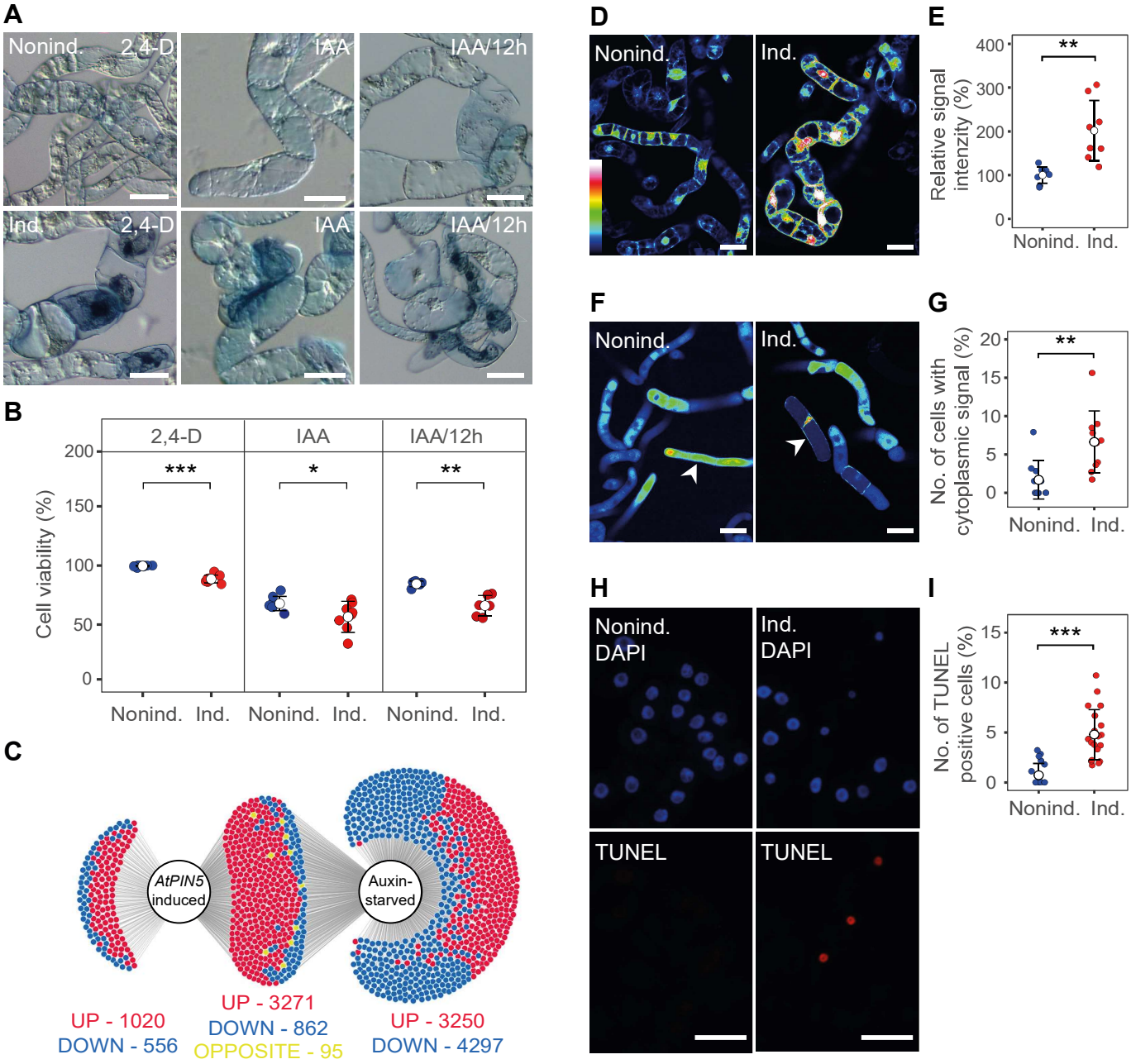
A
Nonind.
2,4-D
IAA
IAA/12h
Ind.
2,4-D
IAA
IAA/12h
B
2,4-D
IAA
IAA/12h
Cell viability (%)
200
150
100
50
0
***
*
**
Nonind.
Ind.
Nonind.
Ind.
Nonind.
Ind.
C
AtPIN5 induced
Auxin-starved
UP - 1020
DOWN - 556
UP - 3271
DOWN - 862
OPPOSITE - 95
UP - 3250
DOWN - 4297
D
Nonind.
Ind.
E
Relative signal intenzity (%)
400
300
200
100
0
**
Nonind.
Ind.
F
Nonind.
Ind.
G
No. of cells with cytoplasmic signal (%)
20
15
10
5
0
**
Nonind.
Ind.
H
Nonind.
DAPI
Ind.
DAPI
TUNEL
TUNEL
I
No. of TUNEL positive cells (%)
15
10
5
0
***
Nonind.
Ind.

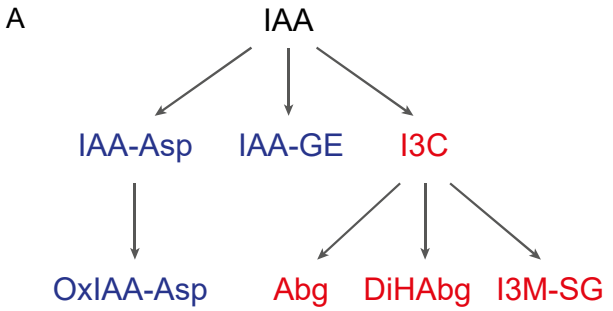
A
IAA
IAA-Asp
IAA-GE
I3C
OxIAA-Asp
Abg
DiHAbg
I3M-SG

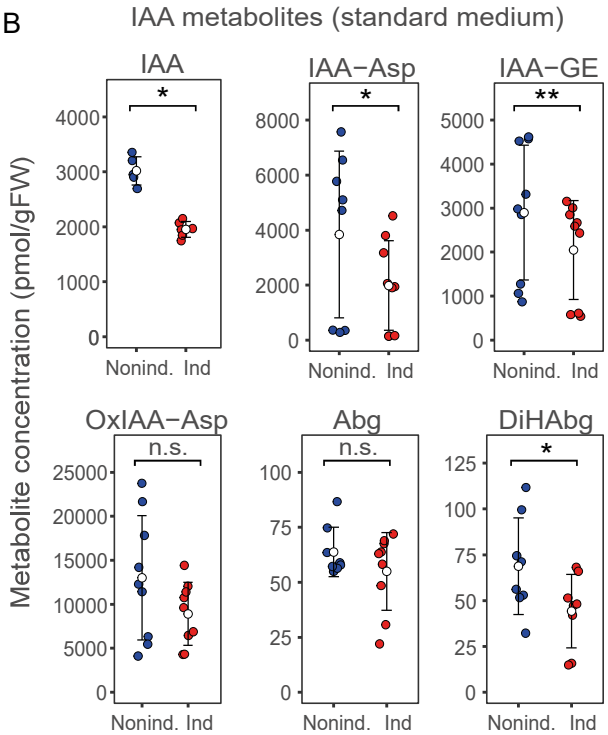
B
IAA metabolites (standard medium)
Metabolite concentration (pmol/gFW)
IAA
IAA−Asp
IAA−GE
OxIAA−Asp
Abg
DiHAbg
Nonind.
Ind
n.s.

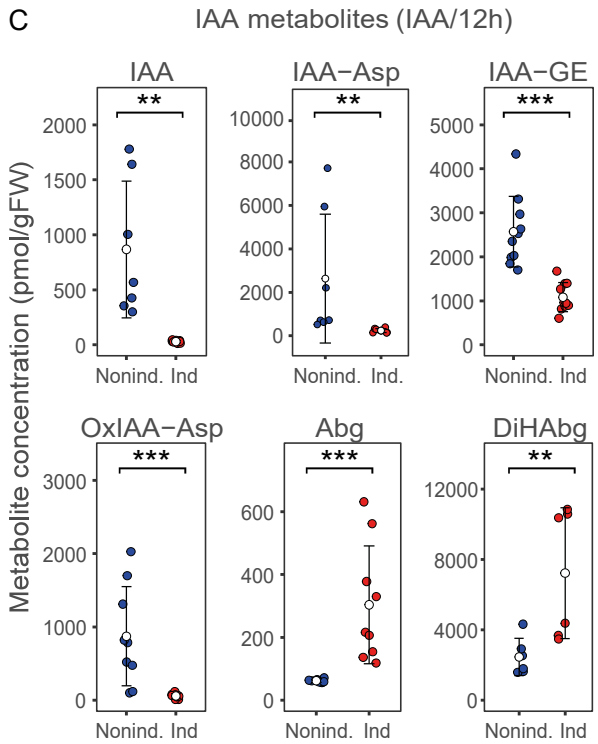
C
IAA metabolites (IAA/12h)
Metabolite concentration (pmol/gFW)
IAA
IAA−Asp
IAA−GE
OxIAA−Asp
Abg
DiHAbg
Nonind.
Ind.
Ind

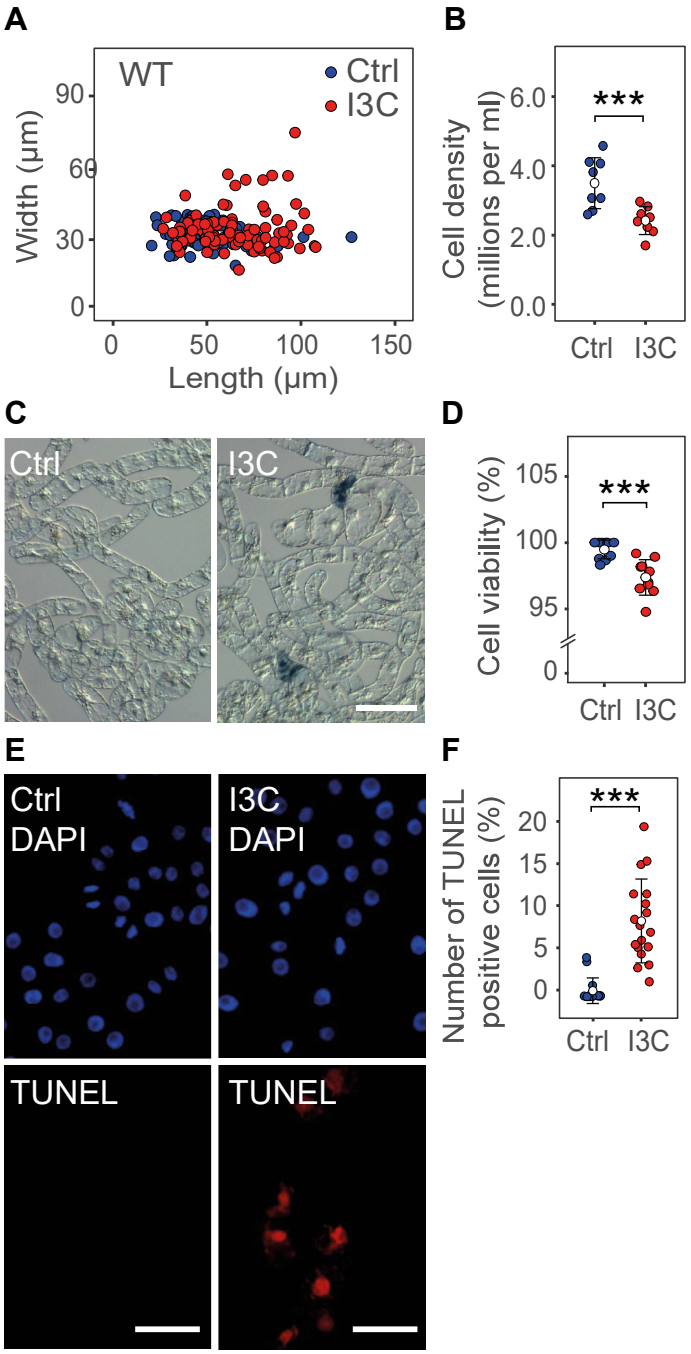
A
WT
Ctrl
I3C
Width (µm)
Length (µm)
0
30
60
90
0
50
100
150
B
Cell density (millions per ml)
***
0.0
2.0
4.0
6.0
Ctrl
I3C
C
Ctrl
I3C
D
Cell viability (%)
***
0
95
100
105
Ctrl
I3C
E
Ctrl DAPI
I3C DAPI
TUNEL
TUNEL
F
Number of TUNEL positive cells (%)
***
0
5
10
15
20
Ctrl
I3C

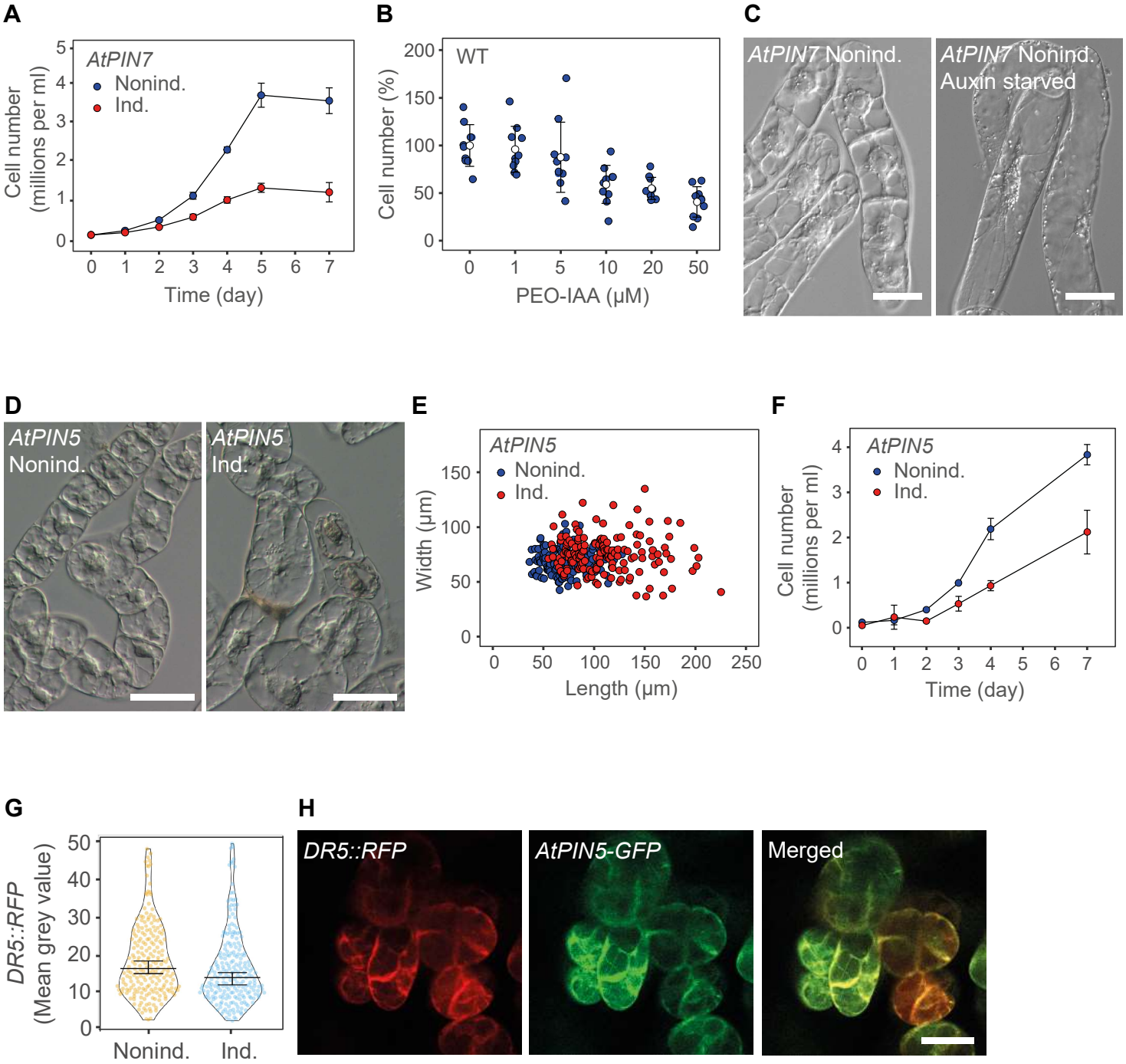
A
AtPIN7
Nonind.
Ind.
Cell number (millions per ml)
Time (day)
B
WT
Cell number (%)
PEO-IAA (μM)
C
AtPIN7 Nonind.
AtPIN7 Nonind. Auxin starved
D
AtPIN5 Nonind.
AtPIN5 Ind.
E
AtPIN5
Nonind.
Ind.
Width (μm)
Length (μm)
F
AtPIN5
Nonind.
Ind.
Cell number (millions per ml)
Time (day)
G
DR5::RFP (Mean grey value)
Nonind.
Ind.
H
DR5::RFP
AtPIN5-GFP
Merged

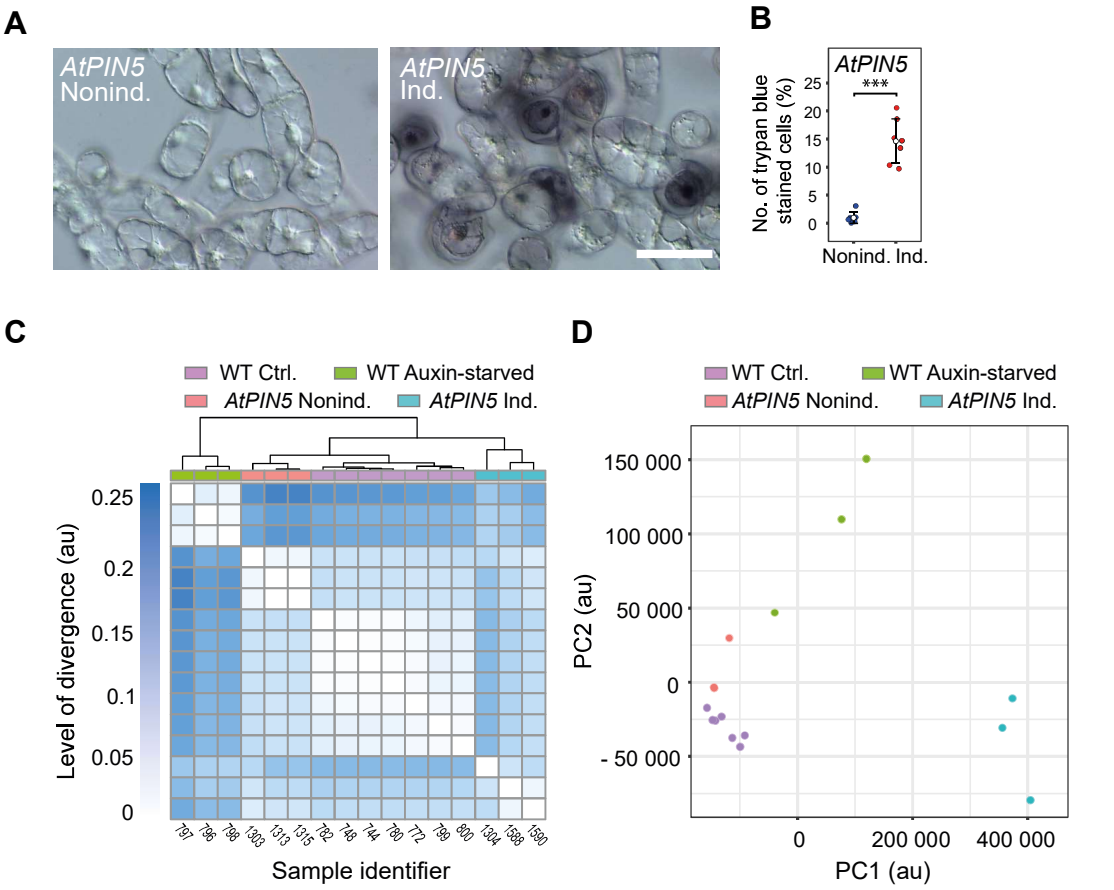
A
AtPIN5
Nonind.
AtPIN5
Ind.
B
AtPIN5
***
No. of trypan blue stained cells (%)
25
20
15
10
5
0
Nonind.
Ind.
C
WT Ctrl.
WT Auxin-starved
AtPIN5 Nonind.
AtPIN5 Ind.
Level of divergence (au)
0.25
0.2
0.15
0.1
0.05
0
797
796
798
1303
1313
1315
782
748
744
780
772
799
800
1304
1308
1590
Sample identifier
D
WT Ctrl.
WT Auxin-starved
AtPIN5 Nonind.
AtPIN5 Ind.
PC2 (au)
150 000
100 000
50 000
0
- 50 000
0
200 000
400 000
PC1 (au)

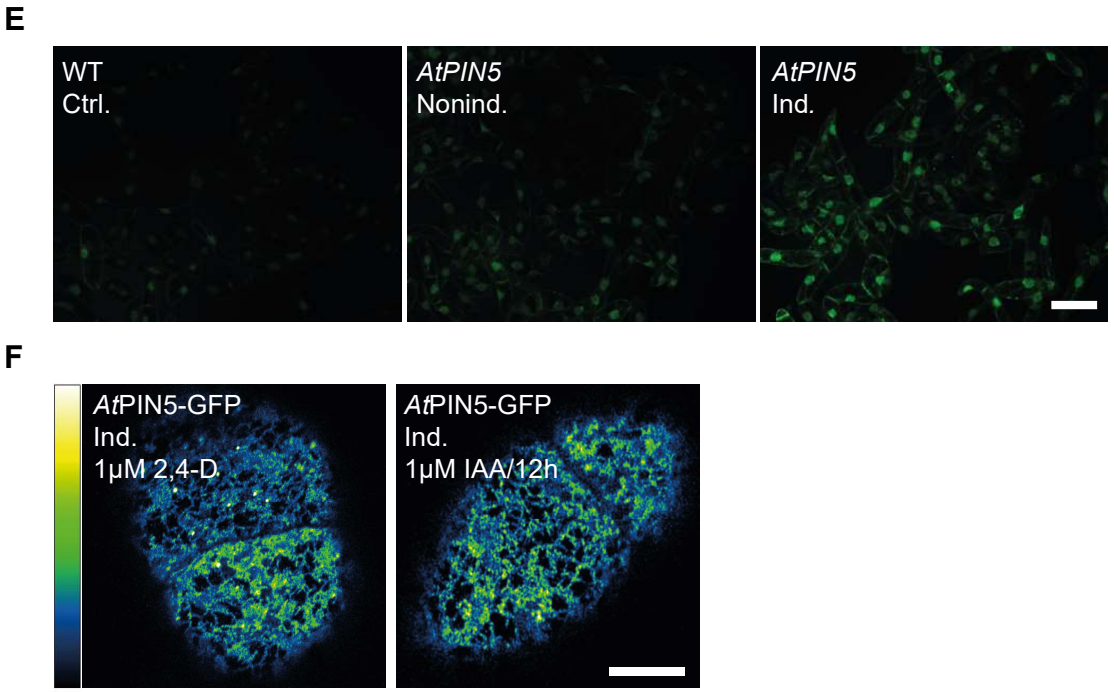
E
WT
Ctrl.
AtPIN5
Nonind.
AtPIN5
Ind.
F
AtPIN5-GFP
Ind.
1µM 2,4-D
AtPIN5-GFP
Ind.
1µM IAA/12h

A

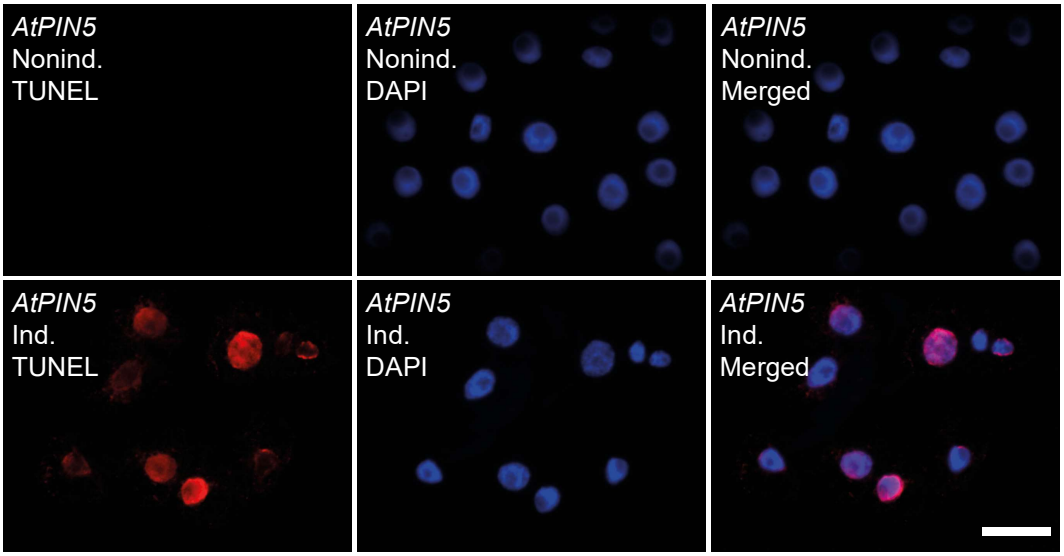
AtPIN5
Nonind.
TUNEL
AtPIN5
Nonind.
DAPI
AtPIN5
Nonind.
Merged
AtPIN5
Ind.
TUNEL
AtPIN5
Ind.
DAPI
AtPIN5
Ind.
Merged

B

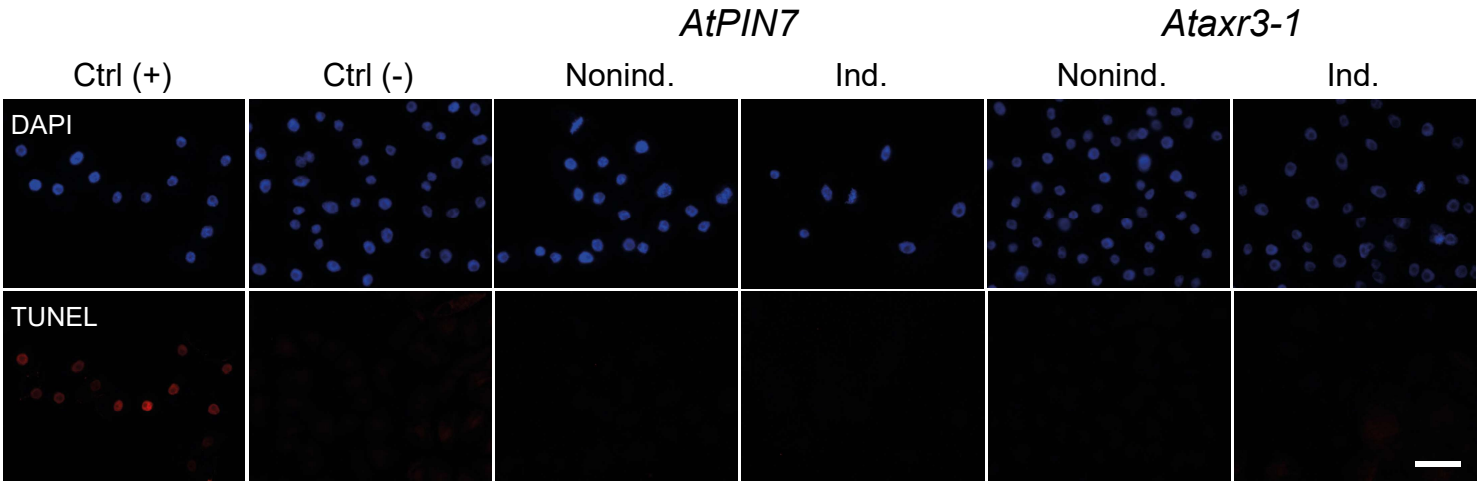
AtPIN7
Ataxr3-1
Ctrl (+)
Ctrl (-)
Nonind.
Ind.
Nonind.
Ind.
DAPI
TUNEL

C

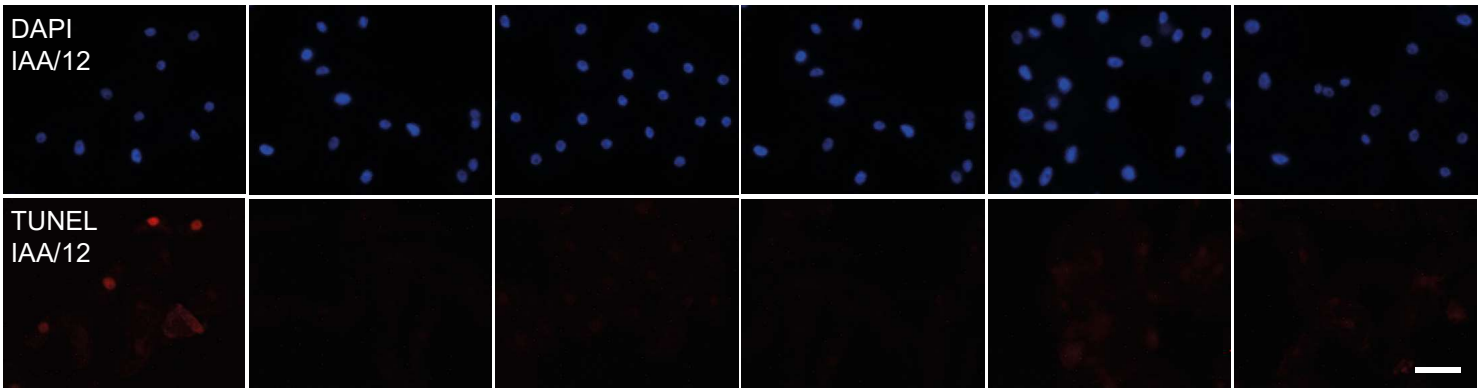
DAPI
IAA/12
TUNEL
IAA/12

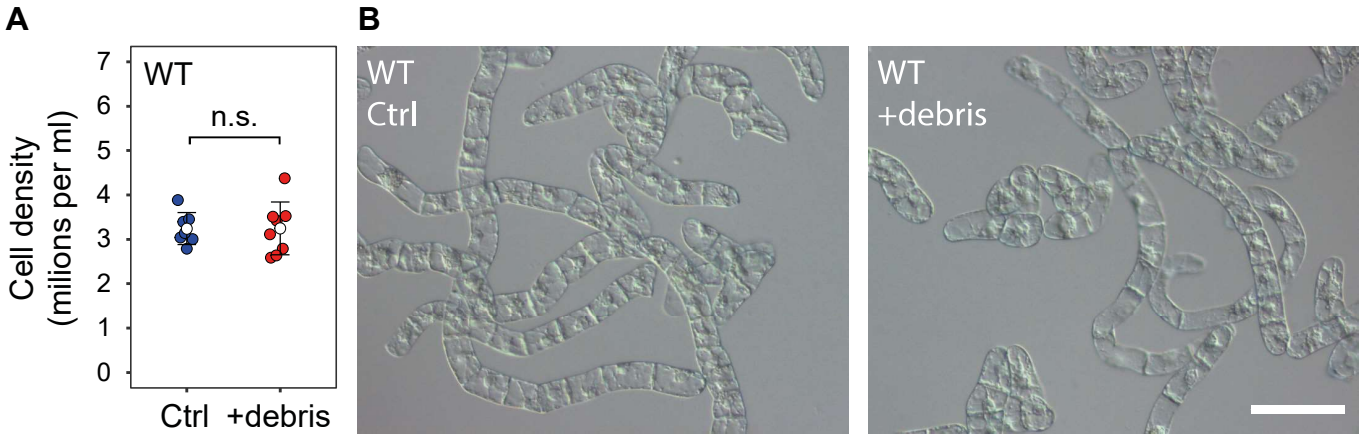
A
B
WT
n.s.
Cell density
(milions per ml)
7
6
5
4
3
2
1
0
Ctrl
+debris
WT
Ctrl
WT
+debris

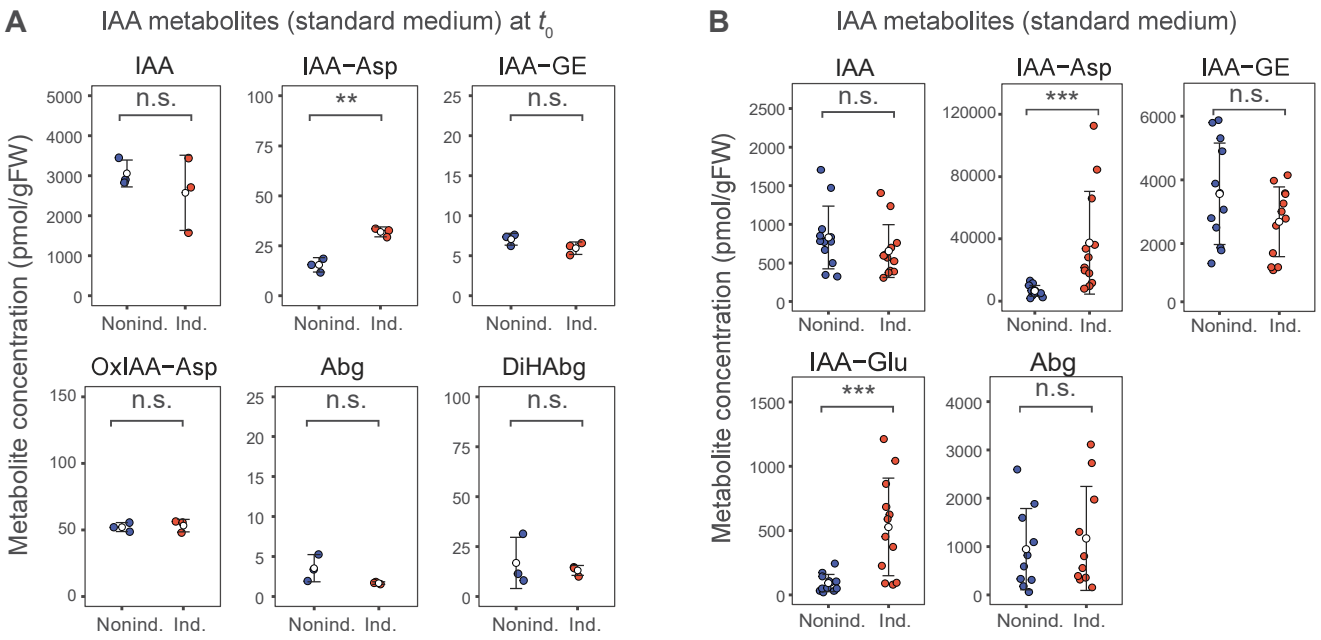
A
IAA metabolites (standard medium) at t_0
IAA
IAA−Asp
IAA−GE
OxIAA−Asp
Abg
DiHAbg
n.s.
**
Metabolite concentration (pmol/gFW)
Nonind.
Ind.
B
IAA metabolites (standard medium)
IAA
IAA−Asp
IAA−GE
IAA−Glu
Abg
n.s.
***
Metabolite concentration (pmol/gFW)
Nonind.
Ind.